

A DIRECT IMAGING SURVEY OF SPITZER DETECTED DEBRIS DISKS: OCCURRENCE OF GIANT PLANETS IN DUSTY SYSTEMS*

TIFFANY MESHKAT^{1,2}, DIMITRI MAWET^{2,3}, MARTA BRYAN³, SASHA HINKLEY⁴, BRENDAN P. BOWLER^{5,†}, KARL R. STAPELFELDT^{2,6}, KONSTANTIN BATYGIN³, DEBORAH PADGETT^{2,6}, FARISA Y. MORALES², EUGENE SERABYN², VALENTIN CHRISTIAENS^{7,8,9}, TIMOTHY D. BRANDT^{10,‡}, ZAHED WAHHAJ¹¹

Draft version November 5, 2018

ABSTRACT

We describe a joint high contrast imaging survey for planets at Keck and VLT of the last large sample of debris disks identified by the Spitzer Space Telescope. No new substellar companions were discovered in our survey of 30 Spitzer-selected targets. We combine our observations with data from four published surveys to place constraints on the frequency of planets around 130 debris disk single stars, the largest sample to date. For a control sample, we assembled contrast curves from several published surveys targeting 277 stars which do not show infrared excesses. We assumed a double power law distribution in mass and semi-major axis of the form $f(m,a) = Cm^\alpha a^\beta$, where we adopted power law values and logarithmically flat values for the mass and semi-major axis of planets. We find that the frequency of giant planets with masses 5-20 M_{Jup} and separations 10-1000 AU around stars with debris disks is 6.27% (68% confidence interval 3.68 - 9.76%), compared to 0.73% (68% confidence interval 0.20 - 1.80%) for the control sample of stars without disks. These distributions differ at the 88% confidence level, tentatively suggesting distinctness of these samples.

Keywords: planets and satellites: detection—techniques: high angular resolution—methods: statistical—circumstellar matter

1. INTRODUCTION

High angular resolution observations utilizing adaptive optics (hereafter “AO”) and coronagraphy allow the study of exoplanets at separations of tens to hundreds of AU, outside of the reach of the transit and radial velocity detection methods. Just as the radial velocity technique revealed an unexpected reservoir of planets in extremely close orbits around their stars, the high-contrast images of HR 8799bcde, β Pic b, HD 95086 b, HD

106906 b, 51 Eri b, and HIP 65426 b (Marois et al. 2010; Lagrange et al. 2010; Rameau et al. 2013a; Bailey et al. 2014; Macintosh et al. 2015; Chauvin et al. 2017), have demonstrated that planets of several Jupiter masses can also exist at astonishingly large orbital distances: ~ 650 AU in the case of HD 106906 b and up to ~ 2000 AU for GU Psc b (Naud et al. 2014). Understanding the true frequency of these objects at wider separations allows planet formation theorists and modelers to fill out the census of planetary mass companions and more fully characterize the orbital architecture of planetary systems. Directly imaging planets opens the door for subsequent spectroscopic study of the planets themselves (Bowler et al. 2010; Barman et al. 2011; Konopacky et al. 2013; Ingraham et al. 2014; Macintosh et al. 2015; Bonnefoy et al. 2016).

Most of the aforementioned directly imaged planets orbit stars with bright debris disks, tenuous dust clouds formed from the ongoing collisions of circumstellar rocky or icy parent bodies. Indeed, based on the presence and structure of the β Pic disk, the existence of the planet β Pic b was predicted well before its discovery (Smith & Terrile 1984; Beust & Morbidelli 2000; Lagrange et al. 2009). Moreover, gravitational stirring by planetary mass companions serves as a driver for the collisional processes which lead to dust production. The presence of a bright debris disk is thus a likely indicator that one or more planetary mass companions are present. Studying the dynamical interactions between planetary mass companions and their debris disks, is an opportunity to better understand the exoplanetary system as whole (Chiang et al. 2009; Boley et al. 2012). These systems are dynamical laboratories where we can study the induced morphology of the disks based on the secular and resonant interactions with perturbing planets (Kennedy & Wyatt 2014; Lee & Chiang 2016;

¹ IPAC, Caltech, M/C 100-22, 1200 E. California Blvd, Pasadena, CA 91125, USA

² Jet Propulsion Laboratory, California Institute of Technology, 4800 Oak Grove Drive, Pasadena, CA 91109, USA

³ California Institute of Technology, 770 S Wilson Ave, Pasadena CA 91125, USA

⁴ University of Exeter, Physics Department, Stocker Road, Exeter, EX4 4QL, UK

⁵ McDonald Observatory and the University of Texas at Austin, Department of Astronomy, 2515 Speedway, Stop C1400, Austin, TX 78712, USA

⁶ Laboratory for Exoplanets and Stellar Astrophysics, Code 667, NASA Goddard Space Flight Center, Greenbelt, MD 20771, USA

⁷ Departamento de Astronomía, Universidad de Chile, Casilla 36-D, Santiago, Chile

⁸ Space sciences, Technologies & Astrophysics Research (STAR) Institute, Université de Liège, Allée du Six Août 19c, B-4000 Sart Tilman, Belgium

⁹ Millennium Nucleus “Protoplanetary Disks in ALMA Early Science”, Chile

¹⁰ Astrophysics Department, Institute for Advanced Study, Princeton, NJ, USA

¹¹ European Southern Observatory, Alonso de Córdova 3107, Vitacura, Casilla 19001, Santiago, Chile

[†] Hubble Fellow

[‡] Sagan Fellow

* Some of the data presented herein were obtained at the W.M. Keck Observatory, which is operated as a scientific partnership among the California Institute of Technology, the University of California and the National Aeronautics and Space Administration. The Observatory was made possible by the generous financial support of the W.M. Keck Foundation.

Nesvold et al. 2016, 2017). The disk shapes and morphologies can help to constrain the masses of any perturbing companions (Morrison & Kratter 2016).

Bowler (2016) performed a meta-analysis on 384 stars with published direct imaging data and found the occurrence rate of giant planets to be $0.6^{+0.7}_{-0.5}\%$, using hot-start planet cooling models. This analysis included all published single stars across the full spectral range, with no additional selection for the presence of a debris disk. In this work, we compile the largest survey thus far of debris disk-selected targets in order to set strict limits on the occurrence of giant planets around stars with debris disks, as compared with a large control sample of diskless stars. We describe our observing campaign targeting the last significant sample of stars with debris disks from the Spitzer Space Telescope. We combine these data with four published deep high contrast imaging surveys of stars with debris disks.

In Section 2, we discuss our target sample selection, observations, data reduction, and present the contrast limits achieved in our Keck and VLT data. In Section 3, we combine our sample with contrast limits from three published surveys (Wahhaj et al. 2013; Rameau et al. 2013b; Janson et al. 2013; Meshkat et al. 2015) and describe the observing strategies from those surveys. We also discuss our selection criteria for the control sample of stars without debris disks. In Section 4, we explain our strategy for single epoch detections, we derive disk properties for our targets based on SED modeling, and we describe how we measure the companion occurrence rate. In Section 5, we discuss how the companion occurrence rates differ between the debris disk and control samples and analyze the planet frequency in the context of our derived disk properties.

2. SPITZER SELECTED TARGETS

The Spitzer Space Telescope has conducted several surveys for debris disks around nearby stars. Although debris disks are more common around younger A stars (Rieke et al. 2005; Su et al. 2006), about 10% of F, G, and K stars show signs of debris disks (Trilling et al. 2008; Carpenter et al. 2009), and these disks are rarer around M stars (Gautier et al. 2007). The presence of a 22 or 24 micron excess in FGK type stars can help to rule out an advanced age for the system (i.e. it is unlikely that an FGK star with a significant excess will be older than ~ 1 Gyr). Thus, for A and FGK stars, warm dust may be an indication of youth.

Results for ~ 600 targets are reported in the above studies, and represent the output of the Spitzer Legacy and GTO programs that were defined early in the mission. The largest remaining Spitzer debris disk survey is a volume-limited study of 600 additional F, G, and K stars within 25 pc of the Sun by (Koerner et al. 2010). Koerner et al. (2010) identified an additional 49 nearby stars with debris disks detected as infrared excess at either 24 or 70 μm . These disks have characteristic fractional infrared luminosities of 0.01 %, and radii of 25 AU that cannot be spatially resolved by Spitzer.

In this work, we observed the 23 stars with the brightest infrared excesses with Keck/NIRC2 and VLT/NACO (see Table 2). We have also included 7 additional nearby stars with known, young ages found to have debris disks from Plavchan et al. (2009), bringing the total number of new targets we observed to 30.

Three more targets were observed at the VLT as part of this survey (HIP 58576, HIP 72848, HIP 74975), however the infrared excess observed in these targets with Spitzer was not confirmed with the WISE instrument (Patel et al. 2014). Thus, we have removed these targets from the following analysis.

Koerner et al. (2010) only provides ages for some of the stars in that sample. Where available, we used literature ages which used a variety of estimation methods including young moving group membership, isochrone fitting, Lithium abundances, and Ca H&K line emission. For targets which had no literature age, we derived the Koerner et al. (2010) ages from their Ca H&K emission line strengths, using the formula from Mamajek & Hillenbrand (2008). For the targets lacking Ca H&K line strengths (HIP 25775, HIP 44295, HIP 77952), we calculated the ages using an empirical relation to convert the excess emission into an age (Rieke et al. 2005).

2.1. Observations

Data were obtained for 17 targets in 2010 (Program ID: C256N2, PI: Sasha Hinkley) and one target in 2012 (Program ID: C248N2, PI: Heather Knutson) with the Keck/NIRC2 instrument (Wizinowich 2013) and 16 targets in 2010 (Program ID: 085.C-0635(A), 086.C-0505(A), PI: Dimitri Mawet) at the Very Large Telescope (VLT)/UT4 with NACO (Lenzen et al. 2003; Rousset et al. 2003).

NACO data were obtained in L' -band with the classical Lyot $0''.7$ diameter coronagraph. NIRC2 data were obtained in Kp -band with the corona300 300 mas diameter) aperture coronagraph. All data were obtained in pupil tracking mode, in order to perform angular differential imaging (ADI; Marois et al. 2006) and PSF subtraction using principal component analysis (PCA; Soummer et al. 2012; Amara & Quanz 2012) on the data. Table 2 contains details about the observations for each of our targets, including observation date, total integration time and on-sky rotation. The observing strategy varied from target to target depending on the conditions on the night. In general, we aimed to obtain more than 15° sky rotation in order to minimize self-subtraction of a potential companion in the post-processing. Some of the targets were observed both with NIRC2 and NACO, to follow-up potential companions. We also obtained short unsaturated off-axis images for photometric calibration for all targets.

2.2. Data Reduction

We subtracted the stellar PSF and speckles in our data by processing the centered data cubes with principal component analysis (PCA: Soummer et al. 2012; Amara & Quanz 2012). This algorithm utilizes the sky rotation around each target, due to observing in pupil tracking mode, in order to model and subtract the stellar PSF and residual speckles. We performed PCA subtraction over the full field of view of our targets, with the star masked out. We detected a few candidate companions, six of which were shown to be consistent with background objects (Figure 4) and five were apparent binaries (Table 1). No new substellar companions were found in our data.

Table 1

Relative astrometry of detected binaries. All targets were observed with VLT/NACO, except for HIP 88745 with Keck/NIRC2.

Name	Date	Sep (")	P.A. (°)	Delta mag
HIP 44295B	2010-04-19	5.13 ± 0.03	179.7 ± 0.4	3.66 ± 0.5
HIP 58576B	2010-04-22	1.13 ± 0.02	334.7 ± 1.0	6.12 ± 0.5
HIP 73633B	2010-04-22	3.85 ± 0.02	5.6 ± 0.4	1.86 ± 0.5
HIP 73633C	2010-04-22	3.96 ± 0.02	4.7 ± 0.4	2.29 ± 0.5
HIP 88745B	2010-09-27	1.19 ± 0.01	314.1 ± 0.5	2.6 ± 0.5

Table 2

Targets observed in our Spitzer sample.

Target	Instrument	Filter	Dates (UT)	T_{int} (min)	N_{images}	Rot(°)	0'25*	0'5	0'75	1'0	2'0	3'0	4'0	5'0
HIP 1368	NIRC2	<i>Kp</i>	2010 Sep 27	65.7	197	35.9	9.1	10.4	11.9	12.9	14.7	14.8	14.7	–
HIP 1499	NIRC2	<i>Kp</i>	2010 Sep 27	30.0	90	25.3	8.9	9.9	11.5	12.6	14.7	14.6	14.7	–
HIP 1598	NIRC2	<i>Kp</i>	2010 Sep 27	47.0	94	21.6	8.6	10.0	11.6	12.6	14.6	14.7	14.6	–
HIP 4148	NIRC2	<i>Kp</i>	2010 Sep 27	40.7	122	22.4	–	10.1	11.6	12.6	14.5	14.7	14.6	–
HIP 5944	NIRC2	<i>Kp</i>	2010 Sep 26	30.0	90	24.2	9.1	10.9	12.4	13.6	15.4	15.6	–	–
HIP 7576	NIRC2	<i>Kp</i>	2010 Sep 26	28.0	70	20.4	8.7	10.6	11.8	13.0	14.1	14.3	–	–
HIP 8497	NIRC2	<i>Kp</i>	2010 Sep 26	35.0	70	22.0	8.9	10.7	12.3	13.3	15.5	15.9	–	–
HIP 17439	NIRC2	<i>Kp</i>	2010 Sep 26	50.0	152	17.7	9.4	10.3	11.9	13.0	15.1	15.2	15.2	–
HIP 19893	NACO	<i>L'</i>	2010 Nov 21	12.5	150	22.4	–	9.0	10.0	10.4	12.3	12.2	12.4	12.5
HIP 25775	NACO	<i>L'</i>	2010 Nov 21	12.5	150	46.4	–	8.1	8.9	8.8	9.4	9.6	9.4	9.5
HIP 30503	NIRC2	<i>Kp</i>	2010 Sep 26	45.5	90	19.7	7.8	9.6	10.9	11.8	14.4	14.8	14.8	–
HIP 30729	NACO	<i>L'</i>	2010 Nov 22	10.5	127	7.5	–	7.1	7.6	7.6	8.2	8.4	8.5	8.6
HIP 32919	NIRC2	<i>Kp</i>	2010 Sep 27	28.5	57	19.7	8.4	10.6	12.1	13.2	14.3	14.4	14.3	–
HIP 36515	NACO	<i>L'</i>	2010 Nov 21	25.0	250	58.9	–	9.1	9.9	10.3	11.1	11.0	11.0	11.1
HIP 36827	NACO	<i>L'</i>	2010 Apr 21	24.0	288	22.7	–	9.1	9.3	9.7	9.9	10.1	10.1	10.1
HIP 42333	NACO	<i>L'</i>	2010 Apr 21	14.0	168	19.7	–	11.8	12.0	12.0	12.1	12.0	12.1	12.1
HIP 43534	NIRC2	<i>Kp</i>	2012 Feb 02	28.0	56	12.5	7.3	9.2	10.7	12.2	13.4	13.5	–	–
HIP 44295	NACO	<i>L'</i>	2010 Apr 19	24.6	296	27.7	–	6.9	7.6	7.9	8.4	9.0	9.0	9.2
HIP 50384	NIRC2	<i>Kp</i>	2012 Feb 02	3.3	109	23.3	7.4	9.3	10.5	11.8	13.2	13.2	–	–
HIP 58451	NACO	<i>L'</i>	2010 Apr 21	33.3	400	69.5	–	8.2	9.4	9.9	10.4	10.4	10.5	10.5
HIP 73633	NACO	<i>L'</i>	2010 Apr 22	14.6	176	19.75	–	9.6	9.7	9.7	9.9	10.1	10.0	10.2
HIP 74702	NACO	<i>L'</i>	2010 Apr 20	10.0	120	9.3	–	8.2	9.4	9.9	10.3	10.4	10.5	10.5
HIP 77952	NACO	<i>L'</i>	2010 Apr 21	18.0	216	33.1	–	9.2	11.0	11.6	13.7	13.8	13.9	13.9
HIP 85561	NACO	<i>L'</i>	2010 Apr 21	7.3	88	5.3	–	7.5	8.3	8.6	8.8	8.7	8.7	8.7
HIP 92919	NIRC2	<i>Kp</i>	2010 Sep 26	32.5	130	17.3	8.7	10.4	12.0	13.0	15.0	15.2	–	–
HIP 102626	NIRC2	<i>Kp</i>	2010 Sep 27	43.3	65	15.5	8.9	10.2	11.5	12.6	14.0	14.0	14.0	–
HIP 105184	NACO	<i>L'</i>	2010 Nov 21	13.8	138	15.5	–	6.3	8.6	9.5	10.6	10.7	10.8	10.8
HIP 108028	NIRC2	<i>Kp</i>	2010 Sep 26	21	70	16.0	8.8	9.8	11.5	12.7	14.7	14.9	–	–
HIP 112190	NIRC2	<i>Kp</i>	2010 Sep 26	32.0	80	22.1	9.2	10.8	12.1	13.3	15.1	15.1	–	–
HIP 117779	NIRC2	<i>Kp</i>	2010 Sep 26	21.3	80	26.6	9.4	10.8	12.3	13.4	14.5	14.7	–	–

* Contrast limits in delta mag achieved from 0'25 to 5'0.

In order to determine the sensitivity of our data, we injected fake companions into the raw data before the image processing. Data from NACO/VLT and NIRC2/Keck were both obtained with coronagraphs, thus we could not use the star itself as a photometric reference PSF. We used an unsaturated, off-axis reference PSF as a photometric calibrator to create fake planets, generated from several reference PSFs for NACO/VLT and NIRC2/Keck individually. We scaled down the flux of the unsaturated PSF and injected fake companion point sources at the 20σ level at three different position angles before PCA processing. Depending on the instrument field-of-view, we ran PCA out to $3'3$ for Keck/NIRC2 and $13''$ for VLT/NACO, measured the resulting signal-to-noise from the fake injected planet, and rescaled our results to 5σ . We took the average signal-to-noise of the fake planets for each of the three position angles in order to determine the 5σ limit. We repeated this process at larger radii in order to map the whole

field of view, increasing in steps of 3 resolution elements. We note that for the targets with very little sky rotation ($< 10^\circ$), there is significant self-subtraction at small inner working angles with ADI analysis. We account for this self-subtraction by injecting fake companions into the raw data and measuring the resulting signal-to-noise of the point source after post-processing.

Table 2 lists our 5σ contrast limits from 0'25 and 5'0 from the injected fake planet detection limits. The Keck datasets achieve, on average, better sensitivity due to their increased integration time, on-sky rotation, and the larger aperture size.

3. COMPLETED HIGH CONTRAST IMAGING SURVEYS

We aim to constrain the frequency of giant planets around stars with debris disks by combining our survey results with four samples of debris disk-selected targets, resulting in the largest sample of dusty debris disk stars in direct imaging thus far¹⁵. We combine our Spitzer

¹⁵ Data from on-going large programs such as Morales et al. *in prep*, Gemini Planet Imager Exoplanet Survey, and the SPHERE

dusty debris disk sample (30 targets from Keck and VLT) with published surveys specifically targeting stars with debris disks: the Gemini NICI Planet-Finding Campaign (57 targets, [Wahhaj et al. 2013](#)), the NACO Survey of Young Nearby Dusty Stars (29 targets, [Rameau et al. 2013b](#)), the Strategic Exploration of Exoplanets and Disks with Subaru (41 targets, [Janson et al. 2013](#)), "Holey Debris Disks" survey (15 targets, [Meshkat et al. 2015](#) and Bailey et al. *in prep*). These targets increase the sample size and thus the statistical significance of our analysis. For the targets which have duplicate observations among the surveys, we used the more sensitive contrast curve at 1" in the subsequent analysis. Most contrast curves were presented as 5σ limits, except [Wahhaj et al. \(2013\)](#) and [Janson et al. \(2013\)](#) which we modified to be consistent with 5σ (detailed below). We note that, after subtracting off the stellar contribution using classical ADI and/or PCA, the distribution of noise in the image is approximately Gaussian (see e.g. [Mawet et al. 2014](#)). Thus, we have 130 individual stars in total (binaries have been removed). Table 3 shows the complete target list. The debris disk-selected surveys are discussed in detail below.

3.1. The Gemini-NICI Planet-Finding Campaign

[Wahhaj et al. \(2013\)](#) used the Gemini/NICI instrument to search for exoplanets around young stars with debris disks. Targets were selected based on the presence of an infrared excess. Data were obtained in ADI mode with H and angular spectral differential imaging (ASDI) mode on and off the CH_4 narrow band. Several companion candidates were detected, most were shown to be consistent with background stars. Some of the companion candidates were not followed up and remain single epoch companion candidates. Using Bayesian analysis with flat priors, they find that less than 20% of stars with debris disks have companions more massive than $3 M_{Jup}$ beyond 10 AU. They conclude that systems like β Pic and HR 8799 are likely rare. Contrast curves are presented as a 95% completeness threshold which corresponds to a source bright enough to be detected if it were located on 95% of the background fluctuations, assuming a 3σ minimum for follow-up. Given that a Gaussian distribution with zero mean has 95% of its probability above 1.64σ , a 4.64σ source would be detected at 3σ or better, 95% of the time. We therefore convert the 95% limits to 5σ by subtracting $2.5 \log(4.64/5) \approx 0.081$ mag, and proceed to include the modified sensitivity curves in the remainder of our analysis.

Table 3
Properties of our debris disk sample

Target	R.A.	Dec.	Sp. Type	Dist. (pc)	Age (Myr)	Age Ref	Assoc.	V (mag)	H (mag)	Survey
HIP544	00 06 36.785	+29 01 17.40	K0V	13.7±1.0	200 ⁺¹⁰⁰ ₋₅₀	LS06; 1	HL	6.13±0.05	6.13±0.05	R13
HIP560	00 06 50.087	-23 06 27.14	F3V	39.1±1.0	12 ⁺² ₋₂	Z04; 1	BP	6.17±0.01	6.173±0.01	W13
HIP682	00 08 25.746	+06 37 00.49	G2V	39.1±1.0	90 ⁺¹³⁰ ₋₆₅	A08; 6	-	7.59±0.01	7.59±0.01	J13
HIP1079	00 13 26.664	+27 02 38.46	G2V	34.0±19.0	12 ⁺² ₋₂	Z04; 1	BP	8.7±0.01	8.7±0.01	W13
HIP1368	00 17 06.375	+40 56 53.87	M0.5V	15.0±1.0	295 ⁺²⁰⁵ ₋₁₅	C14; 5	-	9.0±0.02	9.0±0.02	TW – Keck
HIP1481	00 18 26.122	-63 28 38.98	F8V	41.0±1.0	30 ⁺¹⁵ ₋₁₅	Z04; 1	TH	7.46±0.01	7.46±0.01	W13
HIP1499	00 18 41.867	-08 03 10.80	G3V	23.2±1.0	4700 ⁺²⁹⁰⁰ ₋₃₉₃₀	C11; 2,7	-	6.46±0.05	6.46±0.05	TW – Keck
HIP1598	00 20 00.409	+38 13 38.64	G1V	24.8±1.0	2490 ⁺²⁶⁵⁰ ₋₁₈₀₀	C11; 2,7	-	7.07±0.05	7.07±0.05	TW – Keck
HIP4148	00 53 01.135	-30 21 24.90	K2.5V	14.2±1.0	6000 ⁺⁴⁰⁰⁰ ₋₄₁₄₀	C11; 2,7	-	7.17±0.05	7.17±0.05	TW – Keck
HIP5944	01 16 29.253	+42 56 21.90	G0-V	23.2±1.0	462 ⁺³⁵ ₋₃₅	P09; 3,4,5	-	6.59±0.01	6.59±0.01	J13
HIP6276	01 20 32.268	-11 28 03.74	G9V	35.1±1.0	70 ⁺²⁵ ₋₂₅	Z11; 1	ABD	8.39±0.01	8.39±0.01	R13
HIP6878	01 28 34.360	+42 16 03.68	F8	34.8±1.0	250 ⁺¹⁵⁰ ₋₁₅₀	Me09; 6,8	-	6.66±0.01	6.66±0.01	J13
HIP7345	01 34 37.779	-15 40 34.90	A1V	61.0±1.0	40 ⁺¹⁰ ₋₁₀	Z12; 1	-	5.61±0.01	5.61±0.01	W13
HIP7576	01 37 35.466	-06 45 37.53	K0/1V	24.0±1.0	3000 ⁺³⁰⁰⁰ ₋₂₄₀₀	C11; 2,7	HL	7.66±0.05	7.66±0.05	TW – Keck
HIP7805	01 40 24.067	-60 59 56.63	F11V/V	67.0±2.0	30 ⁺¹⁵ ₋₁₅	Z04; 1	TH	7.61±0.01	7.61±0.01	W13
HIP8241	01 46 06.263	-53 31 19.33	A1V	57.0±1.0	346 ⁺¹⁰⁰ ₋₁₀₀	R07; 1,2	UM	5.03±0.01	5.03±0.01	W13
HIP8497	01 49 35.103	-10 41 11.07	F0V	23.2±1.0	830 ⁺¹⁶⁰ ₋₃₀₀	C11; 2,7	-	4.68±0.05	4.68±0.05	TW – Keck
HIP9141	01 57 48.978	-21 54 05.34	G4V	40.9±1.0	30 ⁺¹⁵ ₋₁₅	Z11; 1	TH	8.06±0.06	8.06±0.07	J13
HIP10184	02 10 55.964	+05 05 05.77	G5V	24.4±18.0	1210 ⁺¹⁰⁰⁰ ₋₅₀₀	TW; 4,9	-	9.05±0.02	9.05±0.02	TW – VLT
HIP10409	02 14 06.394	+61 41 03.77	M1V	9.9±11.0	12 ⁺² ₋₂	P09; 1	BP	8.21±0.05	8.21±0.05	J13
HIP10626	02 16 47.379	+43 46 22.79	K2V	52.2±1.0	25 ⁺⁸ ₋₈	P09; 2	-	7.6±0.01	7.6±0.01	TW – Keck
HIP10947	02 21 00.939	-74 00 00.02	F6V	45.1±7.0	30 ⁺¹⁵ ₋₁₅	Z11; 1	TH	10.45±0.04	10.45±0.04	R13
HIP11360	02 26 16.245	+06 17 33.19	F4IV	45.2±1.0	12 ⁺² ₋₂	M11; 1	BP	6.8±0.05	6.8±0.05	W13
HIP11847	02 32 55.810	+37 20 01.04	F0	63.5±3.0	12 ⁺² ₋₂	M11; 1	-	7.49±0.01	7.49±0.01	J13
HIP13141	02 49 01.487	-62 48 23.48	A2V	50.7±1.0	540 ⁺⁹⁰ ₋₉₀	M13; 2	-	5.25±0.01	5.25±0.01	W13
HIP14684	03 09 42.288	-09 34 46.58	G8/K0V	40.2±2.0	100 ⁺⁵⁰ ₋₅₀	De15; 1	ABD	8.49±0.02	8.49±0.02	W13
HIP16449	03 31 53.647	-25 36 50.94	A3IV/V	74.0±3.0	30 ⁺²⁰ ₋₁₀	R07; 1,2	TH	6.37±0.01	6.37±0.01	R13
HIP16537	03 32 55.845	-09 27 29.73	K2Vk	3.2±1.0	600 ⁺²⁰⁰ ₋₂₀₀	M08; 5,6	-	3.73±0.05	3.73±0.05	W13
HIP17439	03 44 09.173	-38 16 54.38	K2V	16.0±1.0	3600 ⁺³⁰⁰⁰ ₋₃₀₀₀	C11; 2,7	-	7.0±0.05	6.996±0.05	TW – Keck
HIP18437	03 56 29.376	-38 57 43.81	A0V	10.0±4.0	187 ⁺¹⁵⁰ ₋₁₇₇	R07; 1,2	ABD	6.89±0.01	6.89±0.01	W13
HIP18859	04 02 36.745	-00 16 08.12	F7/8V	19.2±1.0	75 ⁺²⁵ ₋₂₅	A08; 1,6	ABD	5.38±0.05	5.38±0.05	W13
HD281691	04 09 09.737	+29 01 30.62	G8III	73.0±2.0	20 ⁺¹⁰ ₋₁₀	M08; 3,4,5	-	10.68±0.07	10.68±0.07	J13
HIP19893	04 16 01.586	-51 29 11.94	F1V	20.5±1.0	300 ⁺²⁵⁰ ₋₂₅₀	R07; 1,3	-	4.2±0.05	4.2±0.05	W13

Table 3 — Continued

Target	R.A.	Dec.	Sp. Type	Dist. (pc)	Age (Myr)	Age Ref	Assoc.	V (mag)	H (mag)	Survey
HIP76736	15 40 11.556	-70 13 40.38	A1V	77.3±3.0	157 ⁺³⁰⁰ ₋₁₃₇	R07; 2	-	6.42±0.01	6.42±0.01	W13
HIP76829	15 41 11.377	-44 39 40.34	F2/5V	17.5±1.0	225 ⁺⁷⁵ ₋₇₅	R07; 1,3,8	Pl	4.64±0.05	4.64±0.05	W13
HIP77542	15 49 57.748	-03 55 16.34	B9.5V	99.0±9.0	4.5 ^{+0.5} _{-0.5}	R07; 2,5	-	7.12±0.01	7.12±0.01	W13
HIP77952	15 55 08.562	-63 25 50.62	F1V	12.4±1.0	674 ⁺⁷⁶¹ ₋₁₀₀	D15; 2,7	-	2.85±0.05	2.85±0.05	TW – VLT
HIP79977	16 19 29.243	-21 24 13.28	F2/3V	122.7±12.0	8 ⁺³ ₋₃	P12; 1	US	9.11±0.02	9.11±0.02	J13
HIP82587	16 52 58.058	+31 42 06.02	F0V	29.2±1.0	210 ⁺⁷⁰ ₋₇₀	M09; 1,3,8	Pl	5.33±0.01	5.33±0.01	J13
HIP85157	17 24 06.587	+22 57 37.01	A7V	43.0±1.0	100 ⁺¹⁰⁰ ₋₉₀	M06; 2	-	5.72±0.01	5.72±0.01	W13
HIP85340	17 26 22.217	-24 10 31.12	A3	25.7±1.0	1028 ⁺⁴⁰⁴ ₋₁₄₄	D15; 2,7	-	4.15±0.01	4.15±0.01	W13
HIP85561	17 29 06.558	-23 50 10.02	K5V	18.9±1.0	300 ⁺¹⁰⁰ ₋₁₀₀	TW; 4,9	-	9.6±0.05	9.60±0.05	TW – VLT
HIP86305	17 38 05.515	-54 30 01.56	A5IV/V	44.6±1.0	319 ⁺⁵³² ₋₇₆	D15; 2,7	-	5.24±0.01	5.24±0.01	R13
HIP87108	17 47 53.560	+02 42 26.20	A1V	31.5±1.0	245 ⁺⁶⁵ ₋₆₅	R07; 2	-	3.75±0.05	3.75±0.05	W13
HIP87558	17 53 14.185	+06 06 05.12	F4IV-V	31.1±1.0	500 ⁺³⁰⁰ ₋₃₀₀	R07; 3,8	-	5.76±0.01	5.76±0.01	J13
HIP88399	18 03 03.412	-51 38 56.44	F6V	48.1±1.0	12 ⁺² ₋₂	Z01; 1	BP	7.00±0.05	6.02±0.05	R13
HIP90936	18 33 00.917	-39 53 31.28	F5V	36.0±1.0	200 ⁺¹⁰⁰ ₋₁₀₀	R07; 1,3,8	Pl	6.22±0.01	6.217±0.01	W13
HIP92024	18 45 26.900	-64 52 16.54	A7V	29.2±1.0	12 ⁺² ₋₂	Z04; 1	BP	4.77±0.01	4.77±0.01	W13
HIP92919	18 55 53.225	+23 33 23.93	K0V	21.4±1.0	50 ⁺¹⁰ ₋₁₀	P09; 5	-	8.02±0.05	8.019±0.05	J13
HIP93542	19 03 06.877	-42 05 42.39	B9.5V	56.3±1.0	76 ⁺¹²³ ₋₁₅	D15; 2,7	-	4.72±0.01	4.725±0.01	W13
HIP95261	19 22 51.206	-54 25 26.15	A0V	47.7±1.0	12 ⁺² ₋₂	Z04; 1	BP	5.02±0.01	5.02±0.01	W13
HIP95270	19 22 58.943	-54 32 16.97	F6V	50.6±2.0	12 ⁺² ₋₂	Z04; 1	BP	7.04±0.01	7.04±0.01	W13
HIP95619	19 26 56.483	-29 44 35.62	B8.5	69.0±2.0	86 ⁺¹¹⁹ ₋₁₇	D15; 2,7	-	5.64±0.01	5.64±0.01	W13
HIP95793	19 29 00.988	+01 57 01.62	A0IV	61.2±1.0	12 ⁺⁸ ₋₈	R05; 2	-	5.78±0.01	5.78±0.01	J13
HIP99273	20 09 05.215	-26 13 26.53	F5V	53.0±1.0	12 ⁺² ₋₂	Z04; 1	BP	7.18±0.01	7.18±0.01	W13
HIP99711	20 13 59.846	-00 52 00.75	K1/2V	19.3±1.0	560 ⁺¹⁰ ₋₁₀	S05; 2,6	-	7.77±0.05	7.77±0.05	J13
HD192758	20 18 15.790	-42 51 36.30	F0V	62.0±2.0	40 ⁺¹⁵ ₋₁₅	M06; 1	IC	7.03±0.05	7.03±0.05	W13
HIP101800	20 37 49.119	+11 22 39.64	A1IV	7.9±1.0	225 ⁺³¹¹ ₋₄₃	D15; 2,7	-	5.42±0.01	5.42±0.01	W13
HIP107412	21 45 21.905	-12 47 00.07	F5V	39.0±1.0	200 ⁺¹⁰⁰ ₋₁₀₀	N04; 2	-	6.67±0.01	6.67±0.01	W13
HIP107649	21 48 15.751	-47 18 13.02	G2V	9.9±1.0	1300 ⁺¹⁹⁰⁰ ₋₇₀₀	R07; 2	-	5.58±0.05	5.58±0.05	J13
HIP108028	21 53 05.353	+20 55 49.86	K2.5V	23.0±1.0	182 ⁺⁵⁰ ₋₁₀	G12; 2	-	8.15±0.05	8.15±0.05	TW – Keck
HIP112190	22 43 21.302	-06 24 02.96	K3V	21.5±1.0	4260 ⁺¹⁰⁰⁰ ₋₁₀₀₀	TW; 4,9	-	8.13±0.01	8.13±0.01	TW – Keck
Fomalhaut	22 57 39.046	-29 37 20.05	A4V	7.7±1.0	440 ⁺⁴⁰ ₋₄₀	M12; 2,3,8	-	1.16±0.05	1.16±0.05	W13
HR8799	23 07 28.715	+21 08 03.31	F0	39.4±1.0	30 ⁺¹⁵ ₋₁₅	Z11; 1	Co	5.95±0.01	5.95±0.01	R13
HD219498	23 16 05.023	+22 10 34.82	G5	150.0±2.0	300 ⁺²⁰⁰ ₋₁₀₀	C14; 2	-	9.05±0.01	9.05±0.01	R13
HIP115738	23 26 55.956	+01 15 20.19	A2V	49.7±1.0	70 ⁺²⁵ ₋₂₅	Z11; 1	ABD	4.94±0.05	4.94±0.05	R13
HIP116431	23 35 36.153	+08 22 57.43	F0	68.5±3.0	10 ⁺² ₋₂	R07; 1	Pl	7.34±0.01	7.34±0.01	R13
HIP117452	23 48 55.547	-28 07 48.97	A0V	44.0±1.0	70 ⁺²⁵ ₋₂₅	Z11; 1	ABD	4.57±0.05	4.57±0.05	R13
HIP117779	23 53 08.595	+29 01 05.05	K6V	22.5±2.0	150 ⁺¹⁰⁰ ₋₁₀₀	TW; 4,9	-	9.83±0.01	9.83±0.01	TW – Keck

Note. — Age references: A08: Apai et al. (2008), C09: Carpenter et al. (2009), C11: Casagrande et al. (2011), C14: Chen et al. (2014), D15: David et al. (2016a), De15: Desidera et al. (2015), G12: Gontcharov (2012), I10: Isaacson & Fischer (2010), L07: Lafrenière et al. (2007), LS06: López-Santiago et al. (2006), M06: Moór et al. (2006), M08: Mamajek & Hillenbrand (2008), Me09: Metchev et al. (2009), M09: Moór et al. (2009), M10: Maldonado et al. (2010), M11: Moór et al. (2011), M12: Mamajek et al. (2012), M13: Meshkat et al. (2013), M15: Meshkat et al. (2015), N04: Nordström et al. (2004), P09: Plavchan et al. (2009), P12: Pecaut et al. (2012), R07: Rhee et al. (2007), R05: Rieke et al. (2005), S05: Saffe et al. (2005), TW: This work, V12: Vican (2012), Z01: Zuckerman et al. (2001), Z04: Zuckerman & Song (2004), Z11: Zuckerman et al. (2011), Z12: Zuckerman & Song (2012). Age determination methods: (1) cluster/group membership, (2) isochrone fitting, (3), x-ray age correlation, (4) Calcium H&K emission age correlation, (5) rotation age correlation, (6) chromospheric activity, (7) Stromgren photometry, (8) Lithium abundances, (9) Rieke disk-age correlation. Associations: HL: Hercules-Lyra, BP: Beta Pic moving group, TH: Tucana/Horlogium, ABD: AB Dor moving group, UM: Ursa Majoris moving group, G2: Great Austral Young Association, Ar: Argus, Pl: Pleiades moving group, US: Upper-Scorpius, IC: IC2391, Ca: Castor, Co: Columba.

3.2. NaCo Survey of Young Nearby Dusty Stars

The Rameau et al. (2013b) survey targeted young, nearby stars with dusty debris disks searching for giant planets. Data were obtained with the VLT/NACO instrument in L' -band. The presence of debris disks were inferred based on high infrared excesses in 24 and/or 70 μm . The HD 95086 b planet was discovered as part of this survey (reported in Rameau et al. (2013a)). Following Bonavita et al. (2012), they find that the fraction of stars with giant planets (1-13 M_{Jup}) at large separations (1-1000 AU) is 10.8% to 24.8%, at 68% confidence level. This high fraction is likely due to the large bounds which include planet masses and separations to which these data are not sensitive (i.e. 1 M_{Jup} at 1 AU). Data are presented in 5 sigma contrast, and thus not rescaled for our meta-analysis.

3.3. Strategic Exploration of Exoplanets and Disks with Subaru

Janson et al. (2013) use the Subaru/HiCIAO instrument to search for planets and detect scattered light

from debris disk systems. Target selection was based on infrared excesses as well as inferred disk properties from SED modeling such as fractional luminosity and the approximate angular separation. Disks which show the SED signature of a spatially separated warm and cold disk were given priority in the sample. Several companion candidates were detected in this survey and shown to be consistent with background sources. Detection limits are presented at 5.5 sigma, which we modify to 5 sigma contrast by adding $2.5 \log(5.5/5) \approx 0.103$ mag.

3.4. “Holey Debris Disks” survey

Meshkat et al. (2015) and Bailey et al. (*in prep*) obtained data on fifteen young stars which were selected based on membership in young moving groups, and bright debris disks for SED modeling. This project was dubbed the “Holey Debris Disks” survey, based on the holes or gaps in debris disks where the planets are expected to reside. HD 106906 b was discovered by this survey (Bailey et al. 2014) with Magellan AO + Clio2 system. The planetary mass companion ($11 \pm 2M_{\text{Jup}}$) was discovered at a projected separation of $7''.1$ (650 AU). Contrast limits are in 5 sigma, and thus not rescaled for meta-analysis.

3.5. Control Sample

In order to assess the correlation of debris disks with giant, long period planets, we compiled a sample of stars without known debris disks to act as a control sample for our analysis. We included targets from several completed surveys searching for planets (Lafrenière et al. 2007; Vigan et al. 2012; Biller et al. 2013; Nielsen et al. 2013; Brandt et al. 2014; Bowler et al. 2015; Galicher et al. 2016). In order to rule out targets with debris disks, we used several target selections. We removed all stars which overlapped with the targets in this survey, also removed targets from the Wahhaj et al. (2013), Rameau et al. (2013b), Janson et al. (2013), or Meshkat et al. (2015) surveys. We only included targets with J , K_s , $W1$, and $W4$ photometry. A target was considered “diskless” if it had no $W1-W4$ excess. We used conservative cuts for excesses with a stepwise change at $\sim K7$: $W1 - W4 < 0.3$ mag for $J - K_s < 0.8$ mag, or $W1 - W4 < 0.6$ mag for $J - K_s > 0.8$ mag (see Figure 1). Targets with binaries within 100 AU were also excluded from the target list. In total, we have 277 targets in our control sample. All contrast curves are scaled to 5 sigma contrast limit.

Figure 2 and Figure 3 compare the ages and spectral types of the debris disk sample with our control sample. We quantified the differences between these distributions by fitting the ages for each sample using a two Gaussian model. We accounted for the uncertainties in the ages for each star by repeating this model fit 5,000 times, where each time we drew a random age from the Gaussian distribution for each age. This resulted in distributions of best fit heights, widths, and means for a two-Gaussian model of both the control and the debris disk populations. We then compared these distributions of six parameters using their Bayesian Information Criterion (BIC). BIC is defined as follows: $BIC = -2L + k \ln(n)$, where L is the likelihood of the model, k is the number of model free parameters, and n is the number of data

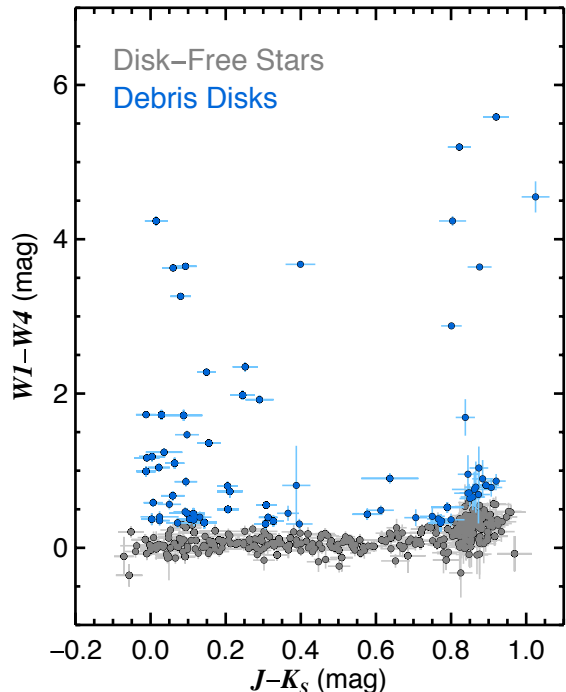


Figure 1. Vetting criteria for the targets included in our disk-free control sample. We included targets from several surveys (Lafrenière et al. 2007; Vigan et al. 2012; Biller et al. 2013; Nielsen et al. 2013; Brandt et al. 2014; Bowler et al. 2015; Galicher et al. 2016) and ruled out those with $W1 - W4 < 0.3$ mag for $J - K_s < 0.8$ mag, or $W1 - W4 < 0.6$ mag for $J - K_s > 0.8$ mag.

points. The lower the BIC value, the better the model fit. Although the likelihood can be increased simply by fitting a more complicated model with more free parameters, BIC selects against these models with a penalty term. When comparing two models, if the delta BIC between them is > 10 , this is strong evidence that the model with the lower BIC value is a better fit (Kass & Raftery 1995). For this model comparison, we fit the combined distributions between the debris disk and control sample populations for heights, widths, and means with a one Gaussian model and a two Gaussian model. We found that for all six parameters the single Gaussian model was preferred (delta BIC > 10), indicating that these age samples are drawn from the same underlying distribution. The increased number of M-stars in the control sample is discussed in Section 4.4 below.

4. RESULTS

4.1. Planetary mass companions

In our debris disk sample, seven planetary mass companions ($< 20 M_{\text{Jup}}$) were discovered or re-detected: HR8799 bcde (Wahhaj et al. 2013; Rameau et al. 2013b), β Pic b (Wahhaj et al. 2013; Rameau et al. 2013b), HD 95086 b (Rameau et al. 2013a), and HD 106906 b (Bailey et al. 2014). The debris disk measurements for these targets are all well-studied and resolved (HR8799; Matthews et al. 2014; Booth et al. 2016, β Pic; Smith & Terile 1984, HD 95086; Su et al. 2015; Moór et al. 2013, and HD 106906; Chen et al. 2005; Kalas et al. 2015). For our statistical analysis, we consider these seven planetary mass companions to be four independent detections, as we treat the HR 8799 four planets as one planetary system detection.

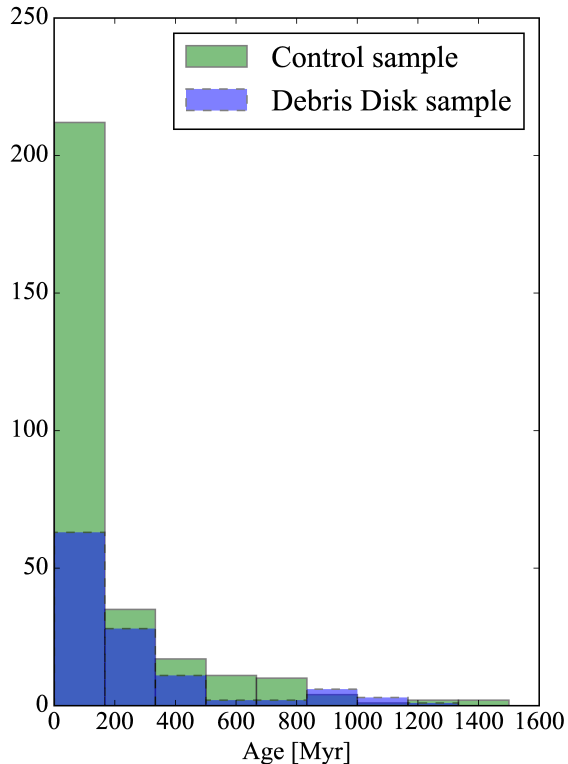


Figure 2. Age distribution for the targets in our debris disk sample (light blue) and the control sample (green). The overlapping regions between these targets is dark blue.

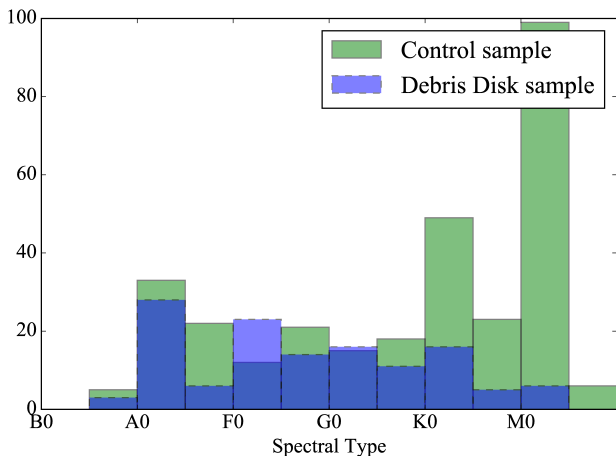


Figure 3. Spectral types for our debris disk sample (blue) and control sample (green).

In the diskless control sample, two planetary mass companion were detected: AB Pic B (Chauvin et al. 2005) and GJ 504 b (Kuzuhara et al. 2013). AB Pic was included as a target in the (Rameau et al. 2013b) dusty debris disk survey, based on the Zuckerman et al. (2011) excess in the $12\mu\text{m}$ IRAS and $24\mu\text{m}$ MIPS/Spitzer channels, suggesting a warm belt. However, no Herschel cold excess was detected and this target has no IRS data. Based on our reanalysis of this target’s SED we conclude that the excess from the warm belt is too tentative to be considered a robust detection of a debris disk. Given the non-detection with Herschel and uncertainty in the presence of a warm belt, we conservatively include AB Pic B in the diskless control sample. The low mass of the

planet GJ 504 b was inferred based on the young age of the star (~ 160 Myr). However, recent reassessments of the age of GJ 504 suggests a much older age (~ 2.5 Gyr; D’Orazi et al. 2016; Fuhrmann & Chini 2015), and thus the companion is more likely to be a 30-40 Jupiter mass brown dwarf. Based on the age reassessment, we do not include this companion as a planetary mass detection in our subsequent statistical analysis. Thus, we have one planetary mass companion ($5\text{-}20 M_{\text{Jup}}$) in the diskless control sample.

4.2. Companion candidates and single epoch detections

We obtained follow-up observations for all point sources detected in our sample of Spitzer selected targets with VLT/NACO and Keck/NIRC2. A few of our sources were found to be likely binaries and thus were not considered for further analysis (see Table 1 for the relative astrometry). The candidate companion around HD 73633 was resolved to be a binary. Six stars showed point sources (HIP 19893, HD 59967, HD 73350, HD 175742, HD 202628, HD 108028; see Figure 4). We confirmed with second-epoch astrometry that all the point sources are not consistent with sharing common proper motion with their host stars, and thus are likely background stars (orbital motion for these widely separated point sources is negligible). The second-epoch data were obtained as part of this program with VLT/NACO, Keck/NIRC2 (HIP 36515, HIP 42333, HIP 92919,), or archival data (VLT/NACO 088.C-0832 for HIP 19893, 089.C-0494 for HIP 105184, and 383.C-0600 for HIP 108028). Table 4 lists the astrometry of these background objects.

Table 4
Astrometry of background objects

Name	Epoch	RA (mas)	σ_{RA}	Dec (mas)	σ_{Dec}
HIP 19893	2011.15	-7142.1	27.0	-3959.0	27.0
	2012.13	-7214.9	27.0	-4165.5	27.0
HIP 36515	2010.39	5541.9	54.0	-4666.7	54.0
	2010.98	5508.6	54.0	-4589.6	54.0
	2011.18	5636.1	30.0	-4580.4	30.0
HIP 42333	2010.31	2352.7	50.0	5334.2	50.0
	2011.18	2660.0	20.0	5266.0	20.0
HIP 92919	2010.82	1907.0	20.0	1809.7	20.0
	2012.74	1637.1	20.0	2320.7	20.0
HIP 105184	2010.97	3983.0	54.0	-3523.8	54.0
	2012.62	3549.1	54.0	-3487.7	54.0
HIP 108028	2009.74	-3008.0	13.0	3137.0	13.0
	2010.82	-2979.0	20.0	3257.0	20.0

Several targets from the published high contrast imaging surveys we included in our complete debris disk and diskless sample have single epoch point source detections. The relative motions of these point sources have not been measured and thus it is not known if these are bound or background objects. For these targets, we follow the conservative strategy in Bowler (2016) and limit the contrast floor to 1σ above the brightest point source reported in the images. Thus, we effectively remove these single epoch detections from our data, in order to prevent their influence on our statistical analysis.

4.3. System Sensitivity Maps

Using a semi-analytical method similar to Brandt et al. (2014), we calculate values for $P_i(m, a)$ as follows:

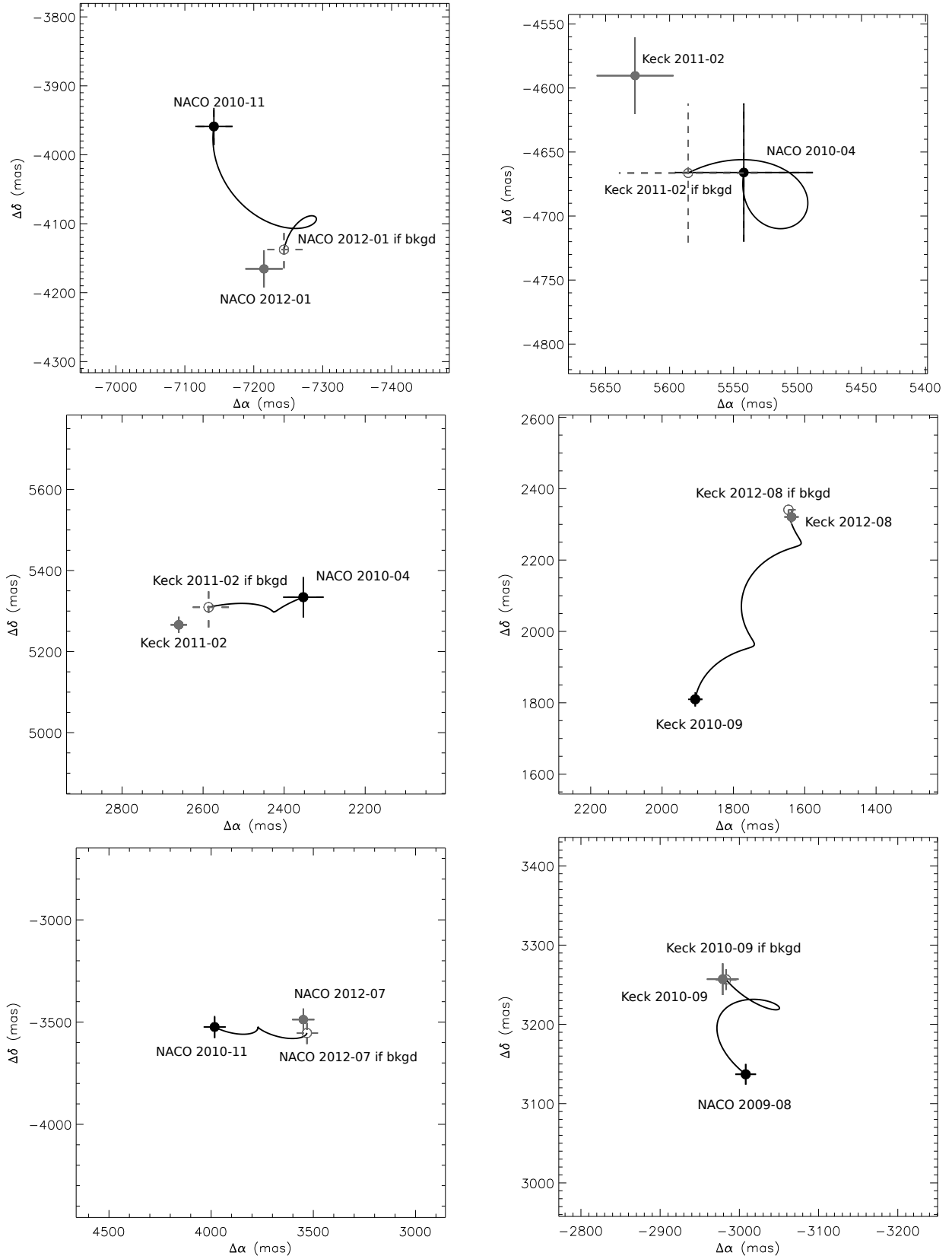


Figure 4. Point sources with proper motion consistent with a background star (Top row Left: HIP 19893, Right: HIP 36515. Middle row Left: HIP 42333, Right: HIP 92919. Bottom row Left: HIP 105184, Right: HIP 108028).

$$P_i(m, a) = \int_0^2 ds p(s) p(m, D = a \times s) \quad (1)$$

where $P_i(m, a)$ is the probability of detecting a companion of mass m at semi-major axis (SMA) a for a given system i , and s is the ratio of the projected separation D over a . We integrate over s from $s = 0$ to $s = 2$, allowing for eccentric orbits which can cause projection effects of up to doubling the SMA. Following the approach in Brandt et al. (2014), $p(s)$ is empirically derived from an eccentricity distribution $p(e)$, uniform up to $e_{\max} = 0.8$. $p(s)$ is well fit by a piecewise linear function:

$$p(s) \approx \begin{cases} 1.3s & 0 \leq s \leq 1 \\ -\frac{35}{32}(s - \frac{9}{5}) & 1 < s < 1.8 \end{cases} \quad (2)$$

The term $p(m, D = a \times s)$ is the probability of detecting a companion of mass m at the projected separation D , and can be computed analytically from the contrast curve $C_i(D)$ as follows:

$$p_i(m, D) = 0.5 + 0.5 \operatorname{erf} \left[\frac{\tau}{\sqrt{2}} \left(\frac{L(m)}{C_i(D)} - 1 \right) \right] \quad (3)$$

where τ is the detection threshold (here $\tau = 5$), $L(m)$ is the luminosity of a companion of mass m , following the COND evolutionary model (Chabrier et al. 2000; Baraffe et al. 2003). $C_i(D)$ is the 1σ contrast curve of object i , function of projected separation D . Because the effective inner working angle of first generation surveys is usually large ($> 5\lambda/D$, where λ is the observing wavelength and D is the telescope diameter), we chose not to correct for small sample statistics (Mawet et al. 2014). For the sake of continuity and comparison with previous studies, we chose to use the COND evolutionary model from Baraffe et al. (2003). The COND03 models were used in order to allow direct comparison with previous analyses (Janson et al. 2013; Rameau et al. 2013b; Bowler 2016; Galicher et al. 2016). However, as noted by Bowler (2016), the COND model is part of hot-start model family, which begin with arbitrarily large radii and oversimplified, idealized initial conditions. It ignores the effects of accretion and mass assembly. The COND model represents the most luminous and thus optimistic outcome. We included the age uncertainties by drawing 10 samples from the age distributions and generating a detection probability map for each age sample. We take the average of these maps to be the final detection probability maps for each target (see Section 3 for discussion about the age distributions).

4.4. Companion occurrence rate

While radial velocity surveys have constrained the mass and semi-major axis (SMA) distributions of gas giant planets at small and intermediate separations (i.e., Cumming et al. 2008; Bryan et al. 2016), direct imaging surveys present a unique opportunity to constrain the occurrence of gas giant planets at wide separations. We determine the occurrence rate of substellar companions around our sample of debris disk stars following methods outlined in Bowler et al. (2015). In short, these survey results can be characterized as Bernoulli trials. While

the number of detections is simply the number of substellar companions detected in these surveys, the number of trials, i.e. the number of times we asked whether we had a detection or non-detection, is given by the sum of sensitivities over a range of mass and semi-major axis and over the sample of systems. Here, the number of trials is given by the following equation:

$$n = \frac{\sum_{i=1}^{N_t} \sum_{j=1}^{N_a} \sum_{k=1}^{N_m} P_i(m_k, a_j)}{N_a N_m} \quad (4)$$

where N_t is the number of systems, N_a is the number of grid points in the specified SMA range, N_m is the number of grid points in the mass range. For this equation we adopt a double power law distribution of the form $dN/(d \log m d \log a) \propto m^\alpha a^\beta$, and assume logarithmically flat distributions of m and a with α and β equal to 0. We note that given the low number of companion detections at wide separations by direct imaging surveys, it is still unclear what distribution their masses and separations follow.

Since these survey results can be characterized as Bernoulli trials, we can model the probability distribution of occurrence rates f as a binomial distribution given by the following equation:

$$P(f|n, k) = \frac{\Gamma(n+1)}{\Gamma(k+1)\Gamma(n-k+1)} f^k (1-f)^{n-k} (n+1) \quad (5)$$

In this equation, n is the number of trials, and k is the number of successes, i.e. the number of detected planets in a given range of mass and SMA. Here we generalize the binomial distribution by generalizing the binomial coefficient using Gamma functions in order to account for non-integer trials.

We calculate the occurrence rate for the debris disk sample over the mass range $5 - 20M_{\text{Jup}}$ and the SMA range 10 - 1000 AU, where we are relatively complete (see Figure 5), which includes detections in systems HR 8799, HD 95086, β Pic, and HD 106906. For the control sample of stars without debris disks, there was one reported companion, AB Pic B (see Section 4.1).

We find the occurrence rate of companions around stars with debris disks is 6.27% with a 68% confidence interval of 3.68 - 9.76% for the range $5 - 20M_{\text{Jup}}$ and 10-1000 AU. For the control sample of diskless stars, the occurrence xfrate is 0.73% with a 68% confidence interval of 0.20 - 1.80%. These distributions differ at the 88% confidence level¹⁶. We also calculated BIC values to compare these populations. We fit the combined distribution, the sum of the two binomial distributions, with one and two binomial distribution models, and calculated the BIC values from these model fits. The two binomial distribution model was highly preferred ($\Delta BIC > 10^4$) in comparison to the single binomial distribution model, suggesting that these two populations are drawn from different distributions. These results hint at a higher occurrence of giant planets around stars with debris disks than those without debris disks. We note that although our statistical formalism handles the detection of only

¹⁶ In this work we list the confidence level rather than sigma since these posterior distributions are skewed and not Gaussian.

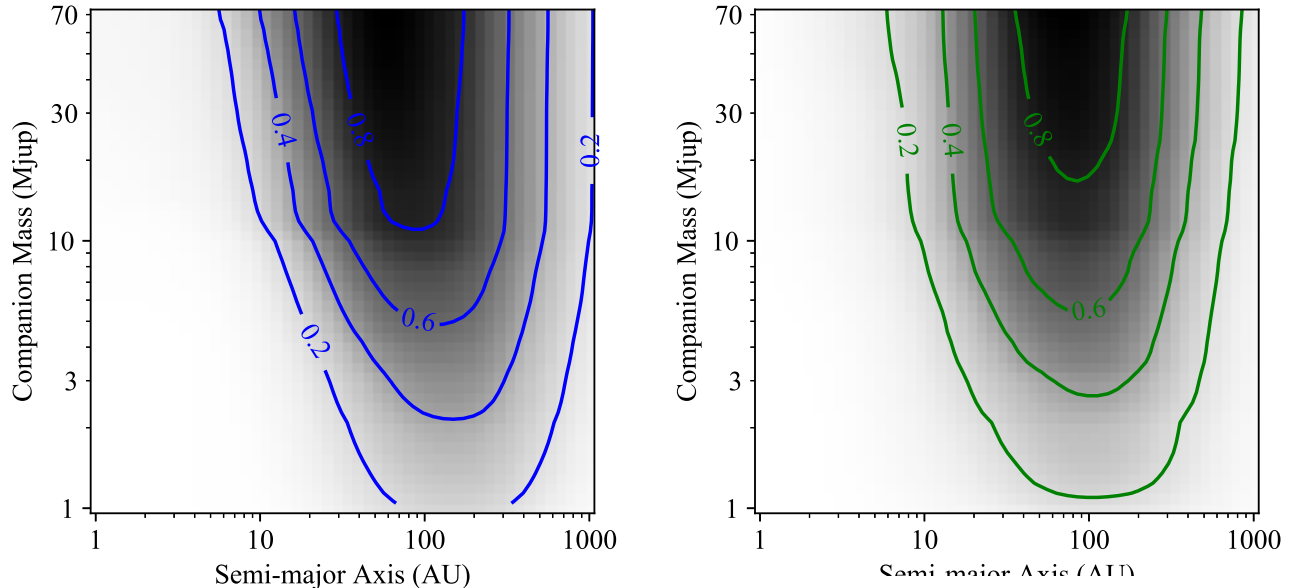


Figure 5. Detection probability map with contours showing the 20, 4 the control sample (right) assuming hot-start and the Baraffe et al. (2006)

one companion around a star at a time, our inclusion of the HR 8799 four-planet system as one planetary system detection demonstrates that this occurrence rate applies to at least one companion per star.

Table 5
Occurrence Rates for Companions (5-20 M_{JUP} and 10-1000 AU) at the 68% confidence level (CL).

	Debris Disk	Control Sample
Full Sample	6.27%, 68CL 3.68-9.76%	0.73%, 68CL 0.20-1.80%
Early-type	9.94%, 68CL 5.82-15.16%	-, 68CL 0-4.17%
Late-type	-, 68CL 0-4.61%	2.18%, 68CL 0.57-5.22%

We repeat these simulations with the early and late-type stars separately, to determine if the measured difference in occurrence rates among debris disk stars is the same or more prominent when considering only high-mass or low-mass stars. For the early-type stars, we find that an occurrence rate for the debris disk sample of 10.1% with a 68% confidence interval of 5.9 - 15.3% and the control sample has a 68% confidence level upper limit of 3.3%, since there were no detections in this sub-sample. For the late-type stars only, we find an occurrence rate for the debris disk sample is a 68% confidence level upper limit of 4.5% and the control sample of 2.1% with a 68% confidence interval of 0.6 - 5.0%. The early-type occurrence rates differ at the 83% confidence interval, and the late-type occurrence rates are consistent at the 68% level. Table 5 summarizes the occurrence rates for the debris disk and control samples, including the full sample of stellar types, as well as sub-samples of early- and late-type stars. The listed rate is the maximum of the probability distribution. Figure 6 shows the probability distributions comparing the debris disk sample and the control sample with the 68% confidence interval shaded. We also calculated these occurrence rates using the power law distribution from Clanton & Gaudi (2016) using the Monte Carlo technique. We found these

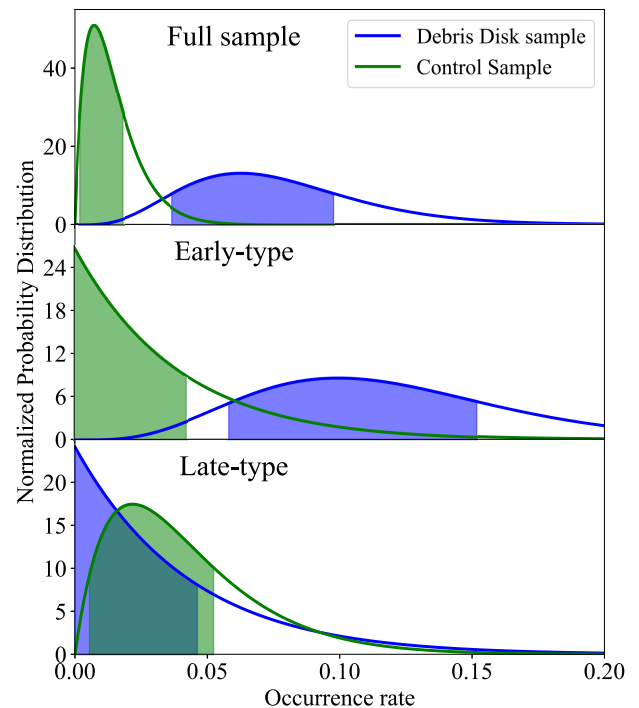


Figure 6. Normalized probability distributions for the debris disk and control samples for the full sample (top), early-type stars only (middle) and late-type stars only (bottom), with the 68% confidence interval shaded.

general occurrence rate trends to be consistent, and thus these results do not depend strongly on our choice of assumptions or priors.

Finally, we perform simulations on the control sample alone to ensure that it is not skewed by the large number of M stars (Figure 3). We repeat the simulations for the control sample without the M stars. The occurrence rate for the control sample without the M-stars is 1.2% with a 68% confidence interval of 0.3 - 2.8%. The non-M star control sample and the control sample occurrence rates

are consistent at the 68% level, thus we can conclude that the disproportionate number of M stars in the control sample in comparison to the disk sample does not bias the derived occurrence rates. When the control sample without M-stars is compared with the debris disk sample, the samples still do not overlap at the 68%. Our test shows that the control sample is minimally biased by the large number of low mass stars.

5. DISCUSSION

We performed our analysis on the complete sample of stars, as well as early- and late-type stars separately. For the complete sample of stars, our simulations hint at a higher occurrence rate for giant planets around stars with debris disks, as these samples differ at the 88% confidence level. When considering only the early-type stars, we also find a higher occurrence rate of giant planets around stars with debris disks (77%). This is consistent with predictions (Zuckerman & Song 2004; Wyatt 2005) that debris disks are the products of giant planets stirring and causing dust collisions, though these results suggest the need for more data to have stronger significance.

The structure and replenishment of a debris disk is often attributed to an eccentric perturbing planet, interior to the debris belt (Wyatt 2005; Chiang et al. 2009; Boley et al. 2012; Nesvold & Kuchner 2015). Nesvold et al. (2016) considered the scenario of a debris disk being shaped by a perturbing planet external to the debris disk. An inclined planet can excite the disk eccentricities with the Kozai-Lidov mechanism. This suggests that the companion responsible for maintaining a debris disk structure may be further separated from its star, and thus easier for direct imaging discoveries. Brown dwarf companions have been directly imaged orbiting exterior to debris disks (i.e., HR3549; Mawet et al. 2015). Out of the planetary mass companions ($< 20M_{\text{Jup}}$) discussed in this work, only HD 106906b orbits external to its debris disk. Nesvold et al. (2017) use collisional and dynamical simulations to model the interactions between the planet HD 106906 b and the debris disk. They find that the planet can be responsible for the disk shape, and thus may have formed in situ (external to the debris disk). More generally, Lee & Chiang (2016) demonstrate through disk modeling how the interaction between a single eccentric planet could produce a variety of observed disk morphologies. Our results are consistent with the theory that debris disks are the result of perturbing companions exciting collisions between dust, however we have too few companion detections to conclude whether the debris disks in our sample are shaped by an internal or external perturber.

In this paper we limited our data to published surveys, which does not include the large, ongoing, second generation data from the GPI Exoplanet Survey (Macintosh et al. 2014) and the SPHERE GTO (Beuzit 2013), as these are not yet completed. One test for those survey results would be to repeat the analysis here, and to adjust the SMA radii range based on the debris disk gap location. This will contribute to our understanding of whether the planet perturbers are present more often around stars with debris, and are located inside the debris disks or external (Nesvold et al. 2016). Below, we derive our warm ($\sim 150\text{K}$) debris radius, based on SED fitting, as often inside of our coronagraphic inner working

angle (see Section 5.2 and Table 6). Hence, we cannot perform this adjusted radius test, as we are limited to cold outer dust and by the inner working angle of the first generation direct imaging instruments.

5.1. Comparison to previous results

Although the evidence is building, the degree to which circumstellar debris disks are the tracers of exoplanetary systems is still an unresolved issue, despite being an active area of theoretical work (e.g. Moro-Martín et al. 2007; Krivov 2010). Indeed, in an attempt to understand the correlation between planets and debris disks, exoplanet host stars have been prime targets for space-based infrared observatories such as *Spitzer* and *Herschel* (e.g. Liseau et al. 2010; Dodson-Robinson et al. 2011). However, studies such as these that use large samples from both populations have not produced statistically strong correlations between the two (Bryden et al. 2009).

The availability of the WISE all sky survey (Wright et al. 2010) has made it possible to search for correlations between the Kepler transiting systems and the presence of warm debris dust (Krivov et al. 2011; Ribas et al. 2012; Lawler & Gladman 2012). For example, a transiting planet was discovered orbiting a 5-10 Myr star with a circumstellar disk (David et al. 2016b; Mann et al. 2016). However, the frequency of debris disks in transiting systems is found to be only a few percent. We note that exoplanet host stars for transiting and radial velocity planets are on average older than the targets in our directly imaged sample. From an opposite approach, Morales et al. (2012) use WISE to explore the incidence of warm (12 and/or 22 μm) dust around planet-host stars (independent of planet detection technique), and also found a $\sim 1\%$ excess incidence for main-sequence stars for the WISE detection limits.

On the other hand, those debris disk systems that have significant spectral coverage into the thermal infrared, facilitating detailed SED fits, occasionally show evidence for dust belts organized into structures with both warm and cold thermal dust components (e.g. Kalas et al. 2005; Moro-Martín et al. 2010; Morales et al. 2011; Chen et al. 2014; Ballering et al. 2014). While this is not definitive proof that planetary mass companions are present in the dusty systems, these dynamical structures provide a tantalizing hint of massive bodies responsible for debris sculpting. The work presented in this paper is the most comprehensive step in demonstrating this connection between wide and massive planetary companions and circumstellar debris.

Comparing occurrence rates from other analyses is challenging due to different assumptions made in the occurrence rate calculations, SMA and mass ranges, as well as varying completeness achieved in the data. For our analysis, we chose a conservative mass range where we were most complete (see Figure 5). Bearing these caveats in mind, we compare our occurrence rate for giant planets around stars with debris disks (6.2% with a 68% confidence interval of 3.6 - 9.7%) to the large debris disk-selected surveys included in this paper. Our results are consistent with Wahhaj et al. (2013), who measure an upper limit occurrence rate of 20% (68% confidence level). Rameau et al. (2013b) find an occurrence rate of 10.8-24.8% (68% confidence). The higher occurrence rate found in Rameau et al. (2013b) may be the result of the

smaller sample size and the large selected SMA and mass ranges (1-1000 AU and 1-13 M_{Jup}) where the data are less complete.

5.2. Debris Disk Radii Estimates

In order to place the sensitivity curves derived above in a more physical context, we have calculated approximate disk radii from the observed dust temperature, or temperature upper limit (e.g. [Chen et al. 2005](#); [Hillenbrand et al. 2008](#)). For the non-detections in our paper, these disk radii estimates combined with our contrast limits allow us to constrain the maximum mass of objects that could be present near the disk.

We use the *Spitzer* photometry to estimate the disk temperatures and disk radii. Many of our targets show only infrared excesses at 24 or 70 μm . While this is sufficient to infer the presence of a debris disk, fitting the SED results in only a temperature upper limit and a radius lower limit. For those stars that show infrared excesses at both 24 and 70 μm , we fit a single temperature black body to these excesses, from which we derive a dust temperature. Table 6 shows several of the parameters derived for the sample including the dust temperature, disk radius, and the corresponding Jupiter mass limit for a companion at that radius, based on our contrast curves.

Table 6
Disk properties for targets with 24 and 70 μm excesses

Target	T_{dust} (K)	R_{disk} (au)	R_{disk} (")	M_{Jup} at R_{disk}
HIP 7576	60	49	2.0	8.65
HIP 36827	114	5	0.2	34.5
HIP 42333	45	150	6.3	7.67
HIP 74702	49	80	5.0	3.1

With a derived dust temperature, the disk radius can quickly be calculated. All the estimates for the disk sizes were constructed under the assumption of non-blackbody grains. We used astronomical silicate properties to calculate the grain emissivity and equilibrium temperature assuming each star has the main sequence luminosity appropriate to the spectral types. We assumed the following sizes based on spectral type for the smallest grains, a_{min} , in the dust size distribution for our calculations: A0 is 5 μm , F0 is 4 μm , G0 is 3 μm , K0 is 2 μm , and M0 is 1 μm . These sizes are approximations anchored in previous modeling by members of our team of the Spectral Energy Distributions of debris disks spatially resolved by the Hubble Space Telescope (e.g. [Krist et al. 2010](#); [Golimowski et al. 2011](#)). These assumptions allow us to convert observed temperatures into disk sizes. The disk inner radius always dominates the far-infrared emission, so the disk radii in Table 6 should be thought of as the disk inner edge.

5.3. Theoretical explanation

Over the last two decades, evidence has been marshaled in support of core-nucleated accretion ([Stevenson 1982](#); [Pollack et al. 1996](#)) as a dominant formation mode of giant planets that reside in close proximity to their host stars (e.g. [Fischer & Valenti 2005](#); [Miller & Fortney 2011](#); [Batygin et al. 2016](#)). In contrast, the primary formation channel of more massive, distant bodies continues to be somewhat uncertain, since direct gravitational

collapse ([Boss 1997](#)) remains a distinct possibility at large stello-centric radii, where the natal gaseous nebulae would have been comparatively colder. In this regard, the preference for dusty debris disks to be accompanied by distant giant planets reported herein, points to the presence of refractory material as a marker for giant planet formation.

The young ages of the host stars within our sample open a unique window into the primordial state of planetary systems that host long-period giant planets. In particular, the orbital architectures provide key extrasolar context for the early dynamical evolution of the solar system itself. The detailed orbital structure of the Kuiper belt ([Levison et al. 2008](#)) implies that the outer members of the solar system once occupied a much more compact (probably resonant) configuration, and were surrounded by a $\sim 20\text{-}50 M_E$ debris disk that extended to ~ 30 AU ([Tsiganis et al. 2005](#); [Nesvorný 2015](#)). Accordingly, the systems redetected by our survey likely represent the closest analogs to the young solar system within the currently known extrasolar planetary census.

A closely related point follows regarding the typical evolutionary sequences of giant planet systems. It is generally established that planets should emerge from their protoplanetary disks on nearly circular, co-planar orbits. Subsequently, a large fraction of the giant planet sub-population evolves onto unstable trajectories, allowing planet-planet scattering to ensue, and shape the final orbital distribution ([Rasio & Ford 1996](#); [Beaugé & Nesvorný 2012](#)). Although this narrative reproduces the observed (RV) eccentricity distribution well ([Jurić & Tremaine 2008](#)), the generic physical process that triggers the dynamical instabilities remains unclear ([Lega et al. 2013](#)). To this end, within the framework of the Nice model, angular momentum exchange between the solar systems outer planets and its primordial debris disk is invoked to initialize the transient instability ([Tsiganis et al. 2005](#); [Levison et al. 2011](#)). Accordingly, the results reported herein provide the suggestion towards the potential universality of interactions between planets and debris disks as a mechanism responsible for igniting large-scale dynamical instabilities in planetary systems.

6. CONCLUSIONS

We describe a survey of stars with *Spitzer*-identified debris disks searching for directly imaged planets. We observed these targets with NIRC2/Keck and NACO/VLT and obtained follow-up data to confirm that all point sources in our data are consistent with background sources. We combined these results with the published contrast curves from four imaging surveys which directly target stars with debris disks: [Wahhaj et al. \(2013\)](#); [Janson et al. \(2013\)](#); [Rameau et al. \(2013b\)](#); [Meshkat et al. \(2015\)](#). Taking into account duplicates between the surveys, our sample of stars with debris disks includes 130 stars, 4 of which have planet detections (HR 8799, β Pic, HD 95086, HD 106906). This is the largest unbiased sample of debris disks surveyed for long-period planets to date. In order to assess the occurrence rate of giant planets around stars with debris disks, we also obtained published contrast curves of 277 stars which do not have a debris disk, to act as a control sample. We verified that the age of the control

sample is consistent with that of the debris disk sample, so as not to bias the results if planetary orbits evolve over time. We assume our sample of gas giant planets are distributed in mass and SMA space according to the double power law $f(m,a)=Cm^\alpha a^\beta$. Taking this companion distribution and our survey completeness in account, we find that the occurrence rate of giant planets around stars with debris disks is 6.27% (68% confidence interval 3.68 - 9.76%), compared to 0.73% (68% confidence interval 0.20 - 1.80%). These distributions differ at the 88% confidence level. We ran simulations with the samples divided into early- and late-type stars to compare occurrence rates as a function of stellar mass. Our results show that early-type stars also show giant planet occurrence rates higher than early-type stars without debris disks, differing at the 77% confidence level. The late-type star populations are consistent at below the 68% confidence level. We also ran simulations for the control sample alone without the M-star population, in order to check if the sample is biased by the larger number of M-stars. The occurrence rate for the control sample without the M-stars is consistent with the control sample including the M-stars, and thus the control sample is not biased.

Our comparison of the occurrence rates of gas giant planets between debris disk systems and our control sample suggests a tentative correlation. However, these results are sensitive to the small number of detected planets, thus we need more planetary mass detections and better completeness in mass and SMA to determine if this trend is significant. This work represents the results from first generation instruments. Second generation instruments will thus be needed to better understand the correlation between giant planets and debris disks.

We thank the anonymous referee for helpful comments and suggestions that improved this paper. This work was performed with support from the Exoplanetary Science Initiative at the Jet Propulsion Laboratory, California Institute of Technology, under contract with NASA. Part of this work was carried out at the Jet Propulsion Laboratory, California Institute of Technology, under contract with NASA. This work was performed in part under contract with the Jet Propulsion Laboratory (JPL) funded by NASA through the Sagan Fellowship Program executed by the NASA Exoplanet Science Institute. Support for this work was provided by NASA through Hubble Fellowship grant #HST-HF2-51369.001-A awarded by the Space Telescope Science Institute, which is operated by the Association of Universities for Research in Astronomy, Inc. for NASA, under contract NAS5-26555. The data presented herein were obtained at the W.M. Keck Observatory, which is operated as a scientific partnership among the California Institute of Technology, the University of California and NASA. The Observatory was made possible by the generous financial support of the W.M. Keck Foundation. The Authors wish to recognize and acknowledge the very significant cultural role and reverence that the summit of Mauna Kea has always had within the indigenous Hawaiian community. We are most fortunate to have the opportunity to conduct observations from this mountain. We thank Rahul Patel, Geoff Bryden, Patrick Lowrance, and Grant Kennedy for

detailed discussion about AB Pic.

REFERENCES

- Amara, A., & Quanz, S. P. 2012, *MNRAS*, 427, 948
 Apai, D. et al. 2008, *ApJ*, 672, 1196
 Bailey, V. et al. 2014, *ApJ*, 780, L4
 Ballering, N. P. et al. 2014, *ApJ*, 793, 57
 Baraffe, I. et al. 2003, *A&A*, 402, 701
 Barman, T. S. et al. 2011, *ApJ*, 733, 65
 Batygin, K. et al. 2016, *ApJ*, 829, 114
 Beaugé, C., & Nesvorný, D. 2012, *ApJ*, 751, 119
 Beust, H., & Morbidelli, A. 2000, *Icarus*, 143, 170
 Beuzit, J.-L. 2013, European Planetary Science Congress 2013, held 8-13 September in London, UK. Online at: <http://meetings.copernicus.org/epsc2013/>; http://meetings.copernicus.org/epsc2013i/A_i, id.EPSC2013-954, 8, EPSC2013
 Biller, B. A. et al. 2013, *ApJ*, 777, 160
 Boley, A. C. et al. 2012, *ApJ*, 750, L21
 Bonavita, M. et al. 2012, *A&A*, 537, A67
 Bonnefoy, M. et al. 2016, *A&A*, 587, A58
 Booth, M. et al. 2016, *MNRAS*, 460, L10
 Boss, A. P. 1997, *Science*, 276, 1836
 Bowler, B. P. 2016, *PASP*, 128, 102001
 Bowler, B. P. et al. 2010, *ApJ*, 723, 850
 —. 2015, *ApJS*, 216, 7
 Brandt, T. D. et al. 2014, *ApJ*, 794, 159
 Bryan, M. L. et al. 2016, *ApJ*, 827, 100
 Bryden, G. et al. 2009, *ApJ*, 705, 1226
 Carpenter, J. M. et al. 2009, *ApJS*, 181, 197
 Casagrande, L. et al. 2011, *A&A*, 530, A138
 Chabrier, G. et al. 2000, *ApJ*, 542, 464
 Chauvin, G. et al. 2017, *ArXiv e-prints*
 —. 2005, *A&A*, 438, L29
 Chen, C. H. et al. 2005, *ApJ*, 623, 493
 —. 2014, *ApJS*, 211, 25
 Chiang, E. et al. 2009, *ApJ*, 693, 734
 Clanton, C., & Gaudi, B. S. 2016, *ApJ*, 819, 125
 Cumming, A. et al. 2008, *PASP*, 120, 531
 David, T. J. et al. 2016a, *Nature*, 534, 658
 —. 2016b, *Nature*, 534, 658
 Desidera, S. et al. 2015, *A&A*, 573, A126
 Dodson-Robinson, S. E. et al. 2011, *AJ*, 141, 11
 D’Orazi, V. et al. 2016, *ArXiv e-prints*
 Fischer, D. A., & Valenti, J. 2005, *ApJ*, 622, 1102
 Fuhrmann, K., & Chini, R. 2015, *ApJ*, 806, 163
 Galicher, R. et al. 2016, *A&A*, 594, A63
 Gautier, III, T. N. et al. 2007, *ApJ*, 667, 527
 Golimowski, D. A. et al. 2011, *AJ*, 142, 30
 Gontcharov, G. A. 2012, *Astronomy Letters*, 38, 771
 Hillenbrand, L. A. et al. 2008, *ApJ*, 677, 630
 Ingraham, P. et al. 2014, *ApJ*, 794, L15
 Isaacson, H., & Fischer, D. 2010, *ApJ*, 725, 875
 Janson, M. et al. 2013, *ApJ*, 773, 73
 Jurić, M., & Tremaine, S. 2008, *ApJ*, 686, 603
 Kalas, P. et al. 2005, *Nature*, 435, 1067
 Kalas, P. G. et al. 2015, *ApJ*, 814, 32
 Kass, R. E., & Raftery, A. E. 1995, *JASA*, 90, 773
 Kennedy, G. M., & Wyatt, M. C. 2014, *MNRAS*, 444, 3164
 Koerner, D. W. et al. 2010, *ApJ*, 710, L26
 Konopacky, Q. M. et al. 2013, *Science*, 339, 1398
 Krist, J. E. et al. 2010, *AJ*, 140, 1051
 Krivov, A. V. 2010, *Research in Astronomy and Astrophysics*, 10, 383
 Krivov, A. V. et al. 2011, *MNRAS*, 418, L15
 Kuzuhara, M. et al. 2013, *ApJ*, 774, 11
 Lafrenière, D. et al. 2007, *ApJ*, 670, 1367
 Lagrange, A.-M. et al. 2010, *Science*, 329, 57
 —. 2009, *A&A*, 493, L21
 Lawler, S. M., & Gladman, B. 2012, *ApJ*, 752, 53
 Lee, E. J., & Chiang, E. 2016, *ApJ*, 827, 125
 Lega, E. et al. 2013, *MNRAS*, 431, 3494
 Lenzen, R. et al. 2003, in *Society of Photo-Optical Instrumentation Engineers (SPIE) Conference Series*, Vol. 4841, Society of Photo-Optical Instrumentation Engineers (SPIE) Conference Series, ed. M. Iye & A. F. M. Moorwood, 944–952

- Levison, H. F. et al. 2011, *AJ*, 142, 152
— 2008, *Icarus*, 196, 258
Liseau, R. et al. 2010, *A&A*, 518, L132
López-Santiago, J. et al. 2006, *ApJ*, 643, 1160
Macintosh, B. et al. 2015, *Science*, 350, 64
— 2014, *Proceedings of the National Academy of Science*, 111, 12661
Maldonado, J. et al. 2010, *A&A*, 521, A12
Mamajek, E. E., & Hillenbrand, L. A. 2008, *ApJ*, 687, 1264
Mamajek, E. E. et al. 2012, *AJ*, 143, 72
Mann, A. W. et al. 2016, *ApJ*, 818, 46
Marois, C. et al. 2006, *ApJ*, 641, 556
— 2010, *Nature*, 468, 1080
Matthews, B. et al. 2014, *ApJ*, 780, 97
Mawet, D. et al. 2015, *ApJ*, 811, 103
— 2014, *ApJ*, 792, 97
Meshkat, T. et al. 2013, *ApJ*, 775, L40
— 2015, *ApJ*, 800, 5
Metchev, S. et al. 2009, *ApJ*, 705, L204
Miller, N., & Fortney, J. J. 2011, *ApJ*, 736, L29
Moór, A. et al. 2006, *ApJ*, 644, 525
— 2011, *ApJ*, 740, L7
— 2013, *ApJ*, 775, L51
— 2009, *ApJ*, 700, L25
Morales, F. Y. et al. 2012, *ApJ*, 757, 7
— 2011, *ApJ*, 730, L29
Moro-Martín, A. et al. 2007, *ApJ*, 658, 1312
— 2010, *ApJ*, 717, 1123
Morrison, S. J., & Kratter, K. M. 2016, *ApJ*, 823, 118
Naud, M.-E. et al. 2014, *ApJ*, 787, 5
Nesvold, E. R., & Kuchner, M. J. 2015, *ApJ*, 815, 61
Nesvold, E. R. et al. 2017, *ArXiv e-prints*
— 2016, *ApJ*, 826, 19
Nesvorný, D. 2015, *AJ*, 150, 68
Nielsen, E. L. et al. 2013, *ApJ*, 776, 4
Nordström, B. et al. 2004, *A&A*, 418, 989
Patel, R. I. et al. 2014, *ApJS*, 212, 10
Pecaut, M. J. et al. 2012, *ApJ*, 746, 154
Plavchan, P. et al. 2009, *ApJ*, 698, 1068
Pollack, J. B. et al. 1996, *Icarus*, 124, 62
Rameau, J. et al. 2013a, *ApJ*, 772, L15
— 2013b, *A&A*, 553, A60
Rasio, F. A., & Ford, E. B. 1996, *Science*, 274, 954
Rhee, J. H. et al. 2007, *ApJ*, 660, 1556
Ribas, Á. et al. 2012, *A&A*, 541, A38
Rieke, G. H. et al. 2005, *ApJ*, 620, 1010
Rousset, G. et al. 2003, in *Society of Photo-Optical Instrumentation Engineers (SPIE) Conference Series*, Vol. 4839, Society of Photo-Optical Instrumentation Engineers (SPIE) Conference Series, ed. P. L. Wizinowich & D. Bonaccini, 140–149
Saffe, C. et al. 2005, *A&A*, 443, 609
Smith, B. A., & Terrile, R. J. 1984, *Science*, 226, 1421
Soummer, R. et al. 2012, *ApJ*, 755, L28
Stevenson, D. J. 1982, *Planet. Space Sci.*, 30, 755
Su, K. Y. L. et al. 2015, *ApJ*, 799, 146
— 2006, *ApJ*, 653, 675
Trilling, D. E. et al. 2008, *ApJ*, 674, 1086
Tsiganis, K. et al. 2005, *Nature*, 435, 459
Vican, L. 2012, *AJ*, 143, 135
Vigan, A. et al. 2012, *A&A*, 544, A9
Wahhaj, Z. et al. 2013, *ApJ*, 773, 179
Wizinowich, P. 2013, *PASP*, 125, 798
Wright, E. L. et al. 2010, *AJ*, 140, 1868
Wyatt, M. C. 2005, *A&A*, 440, 937
Zuckerman, B. et al. 2011, *ApJ*, 732, 61
Zuckerman, B., & Song, I. 2004, *ApJ*, 603, 738
— 2012, *ApJ*, 758, 77
Zuckerman, B. et al. 2001, *ApJ*, 562, L87

APPENDIX

Table 7
Properties of the disk-free control sample

Target	R.A.	Dec.	Sp. Type	Dist (pc)	Age (Myr)	V (mag)	H (mag)	Survey
HIP_5191	01:06:26.10	-14:17:46.0	K1	47.3±1.0	150 ⁺⁵⁰ ₋₃₀	9.52±0.05	7.43±0.03	Biller13
CD-58_553	02:42:33.00	-57:39:37.0	K5	50.0±1.0	45 ⁺⁴ ₋₄	11.0±0.07	7.97±0.04	Biller13
HD_19668	03:09:42.29	-09:34:46.5	G0	37.4±1.0	150 ⁺⁵⁰ ₋₃₀	8.49±0.02	6.79±0.04	Biller13
HIP_24947	05:20:38.00	-39:45:18.0	F6	48.3±1.0	45 ⁺⁴ ₋₄	7.38±0.01	6.22±0.03	Biller13
HIP_25283	05:24:30.10	-38:58:10.0	K6	18.0±1.0	150 ⁺⁵⁰ ₋₃₀	9.05±0.04	6.11±0.03	Biller13
HIP_25486	05:27:04.80	-11:54:04.0	F7	27.0±1.0	23 ⁺³ ₋₃	6.3±0.01	5.09±0.03	Biller13
UY_Pic	05:36:56.80	-47:57:52.9	K0	25.1±1.0	150 ⁺⁵⁰ ₋₃₀	7.68±0.06	5.93±0.04	Biller13
BD-13_1328	06:02:21.90	-13:55:33.0	K4	39.0±1.0	150 ⁺⁵⁰ ₋₃₀	10.55±0.05	7.89±0.04	Biller13
AO_Men	06:18:28.20	-72:02:41.4	K4	38.6±1.0	23 ⁺³ ₋₃	9.81±0.07	6.98±0.03	Biller13
AB_Pic	06:19:12.90	-58:03:15.0	K1	46.1±1.0	45 ⁺⁴ ₋₄	9.2±0.09	7.09±0.02	Biller13
HD_45270	06:22:30.90	-60:13:07.1	G1	23.8±1.0	150 ⁺⁵⁰ ₋₃₀	6.51±0.05	5.16±0.03	Biller13
BD+07_1919A	08:07:09.09	+07:23:00.1	K8	35.1±1.0	150 ⁺⁵⁰ ₋₃₀	9.89±0.05	7.32±0.04	Biller13
HD_70573	08:22:49.95	+01:51:33.5	G1	45.7±1.0	250 ⁺⁵⁰ ₋₅₀	8.71±0.05	7.28±0.03	Biller13
DX_Leo	09:32:43.70	+26:59:18.7	K0	17.8±1.0	250 ⁺⁵⁰ ₋₅₀	7.01±0.05	5.24±0.02	Biller13
HD_92945	10:43:28.30	-29:03:51.4	K1	21.4±1.0	150 ⁺⁵⁰ ₋₃₀	7.72±0.05	5.77±0.05	Biller13
V343_Nor	15:38:57.60	-57:42:27.0	K0	38.5±1.0	23 ⁺³ ₋₃	7.98±0.08	5.99±0.03	Biller13
HIP_82688	16:54:08.20	-04:20:24.0	G0	46.7±1.0	150 ⁺⁵⁰ ₋₃₀	7.82±0.01	6.48±0.04	Biller13
HD_159911	17:37:46.50	-13:14:47.0	K4	45.0±1.0	150 ⁺⁵⁰ ₋₃₀	10.02±0.07	7.02±0.05	Biller13
PZ_Tel	18:53:05.90	-50:10:50.0	G9	51.5±1.0	23 ⁺³ ₋₃	8.34±0.04	6.49±0.05	Biller13
HIP_104308	21:07:51.20	-54:12:59.0	A5	70.9±1.0	45 ⁺⁴ ₋₄	6.7±0.01	6.12±0.02	Biller13
HIP_118121	23:57:35.00	-64:17:53.0	A1	47.4±1.0	45 ⁺⁴ ₋₄	4.99±0.01	4.95±0.03	Biller13
TYC_1752-63-1	01:37:23.23	+26:57:12.0	K7	37.0±2.0	150 ⁺⁵⁰ ₋₃₀	10.73±0.09	7.78±0.02	Bowler15
TYC_523-573-1	20:39:54.60	+06:20:11.8	K7.5	38.5±1.0	150 ⁺⁵⁰ ₋₃₀	10.52±0.06	7.35±0.04	Bowler15
V439_And	00:06:36.80	+29:01:17.0	G8	13.7±7.0	250 ⁺⁵⁰ ₋₅₀	6.13±0.05	4.63±0.14	Brandt14
HIP1134	00:14:10.30	-07:11:57.0	F7	47.1±1.0	45 ⁺¹⁰ ₋₁₀	7.32±0.01	6.17±0.04	Brandt14
BD+54_144	00:45:50.90	+54:58:40.0	F8	52.5±2.0	150 ⁺⁵⁰ ₋₃₀	8.6±0.05	6.40±0.03	Brandt14
26_Cet	01:03:49.00	+01:22:01.0	A8	60.1±1.0	50 ⁺¹⁰ ₋₁₀	6.07±0.01	5.51±0.04	Brandt14
BD+04_439	02:46:14.60	+05:35:33.0	F8	54.3±1.0	45 ⁺⁴ ₋₄	7.88±0.01	6.63±0.05	Brandt14
HR_1621	05:01:25.60	-20:03:07.0	B9	60.7±1.0	45 ⁺¹⁰ ₋₁₀	4.89±0.01	5.02±0.03	Brandt14
HIP29067	06:07:55.30	+67:58:37.0	K6	24.5±1.0	5100 ⁺⁵⁰ ₋₅₀	9.75±0.05	6.81±0.03	Brandt14
V1358_Ori	06:19:08.10	-03:26:20.0	G0	49.2±1.0	45 ⁺¹⁰ ₋₁₀	7.95±0.01	6.59±0.02	Brandt14
26_Gem	06:42:24.30	+17:38:43.0	A2	43.6±1.0	45 ⁺¹⁰ ₋₁₀	5.21±0.05	5.07±0.02	Brandt14
V429_Gem	07:23:43.60	+20:24:59.0	K5	25.8±1.0	150 ⁺⁵⁰ ₋₃₀	10.0±0.06	7.03±0.02	Brandt14
V397_Hya	08:19:19.10	+01:20:20.0	G5	22.9±1.0	50 ⁺¹⁰ ₋₁₀	8.35±0.05	6.22±0.04	Brandt14
V405_Hya	09:04:20.70	-15:54:51.0	K3	28.3±1.0	430 ⁺⁵⁰ ₋₅₀	8.76±0.02	6.54±0.05	Brandt14
NLTT_24062	10:20:45.90	+32:23:54.0	K0	47.1±1.0	50 ⁺¹⁰ ₋₁₀	9.18±0.02	7.38±0.02	Brandt14
GY_Leo	10:56:30.80	+07:23:19.0	K2.5	17.3±1.0	720 ⁺⁵⁰ ₋₅₀	7.38±0.06	5.35±0.03	Brandt14
HD95174	10:59:38.30	+25:26:15.0	K2	22.6±2.0	23 ⁺³ ₋₃	8.45±0.02	6.11±0.03	Brandt14
TYC_3825-716-1	11:20:50.50	+54:10:09.0	K7	57.9±1.0	150 ⁺⁵⁰ ₋₃₀	11.91±0.01	8.69±0.04	Brandt14
G_123-7	12:09:37.30	+40:15:07.0	G9	24.5±1.0	50 ⁺¹⁰ ₋₁₀	7.5±0.05	5.70±0.02	Brandt14
HIP63317	12:58:32.00	+38:16:44.0	K0	44.2±1.0	100 ⁺⁵⁰ ₋₅₀	8.63±0.01	6.95±0.02	Brandt14
EQ_Vir	13:34:43.20	-08:20:31.0	K4.5	20.2±1.0	50 ⁺¹⁰ ₋₁₀	9.37±0.07	6.31±0.04	Brandt14
HIP67412	13:48:58.20	-01:35:35.0	G8	37.7±1.0	50 ⁺¹⁰ ₋₁₀	8.51±0.01	6.89±0.04	Brandt14
BD+04_3100	16:02:22.40	+03:39:07.0	G0	82.0±1.0	100 ⁺⁵⁰ ₋₅₀	8.76±0.02	7.52±0.02	Brandt14
HR_6351	17:03:53.60	+34:47:25.0	A5	55.0±1.0	45 ⁺⁴ ₋₄	6.07±0.01	5.68±0.04	Brandt14
HIP87579	17:53:29.90	+21:19:31.0	K2.5	24.4±1.0	1200 ⁺⁵⁰ ₋₅₀	8.49±0.01	6.30±0.02	Brandt14
HIP87768	17:55:44.90	+18:30:01.0	K5	25.0±1.0	100 ⁺⁵⁰ ₋₅₀	9.15±0.05	6.42±0.02	Brandt14
HR_7214	19:03:32.30	+01:49:08.0	A4	54.9±1.0	150 ⁺⁵⁰ ₋₃₀	5.82±0.01	5.36±0.02	Brandt14
HD201919	21:13:05.30	-17:29:13.0	K6	39.0±1.0	150 ⁺⁵⁰ ₋₃₀	10.61±0.05	7.74±0.04	Brandt14
HN_Peg	21:44:31.30	+14:46:19.0	G0	17.9±2.0	250 ⁺⁵⁰ ₋₅₀	5.95±0.01	4.60±0.04	Brandt14
BD+41_4749	23:19:39.60	+42:15:10.0	G8	50.2±1.0	150 ⁺⁵⁰ ₋₃₀	8.93±0.01	7.28±0.02	Brandt14
2MASSJ00120761-1550327	00:12:07.61	-15:50:32.7	K7	95.0±1.0	100 ⁺²⁰⁰ ₋₇₀	9.28±0.07	6.63±0.04	Galicher16
QT_AND	00:41:17.34	+34:25:16.9	K4	41.0±1.0	100 ⁺²⁰⁰ ₋₇₀	9.98±0.04	7.47±0.03	Galicher16
HIP5186	01:06:22.82	+62:45:41.0	A5	65.0±1.0	125 ⁺²⁰⁰ ₋₇₀	6.52±0.01	6.03±0.03	Galicher16

Table 7 — Continued

Target	R.A.	Dec.	Sp. Type	Dist (pc)	Age (Myr)	V (mag)	H (mag)	Survey
GP_PSC	01:07:05.52	+19:09:08.3	K4	48.0±1.0	50 ⁺⁷⁰ ₋₃₀	10.0±0.01	7.70±0.02	Galicher16
HIP6312	01:21:05.27	+64:39:29.3	A2	78.0±2.0	125 ⁺²⁰⁰ ₋₇₀	6.32±0.01	6.16±0.06	Galicher16
HD8907	01:28:34.36	+42:16:03.7	F8	34.0±1.0	600 ⁺⁹⁴⁰⁰ ₋₃₀₀	6.66±0.01	5.49±0.02	Galicher16
HIP8588	01:50:51.97	+11:02:36.2	F2	43.0±1.0	530 ⁺⁴⁰ ₋₄₀	5.92±0.01	5.19±0.03	Galicher16
HIP9892	02:07:18.06	-53:11:56.5	G7	50.0±1.0	45 ⁺⁴ ₋₄	8.65±0.01	6.99±0.04	Galicher16
HD13433	02:10:56.46	-15:18:53.1	A2	163.0±1.0	125 ⁺²⁰⁰ ₋₇₀	8.16±0.05	8.03±0.03	Galicher16
HIP10680	02:17:25.29	+28:44:42.2	F5	39.0±1.0	23 ⁺³ ₋₃	7.0±0.05	5.84±0.03	Galicher16
HIP12964	02:46:45.11	-21:38:22.3	F3	45.0±1.0	1000 ⁺³⁰⁰ ₋₄₀₀	6.47±0.01	5.63±0.02	Galicher16
HIP14232	03:03:30.16	+28:16:11.6	F0	50.0±1.0	625 ⁺⁵⁰ ₋₅₀	6.36±0.01	5.65±0.05	Galicher16
HIP18547	03:58:03.14	+34:48:50.3	A8	61.0±1.0	125 ⁺²⁰⁰ ₋₇₀	6.53±0.01	6.02±0.02	Galicher16
BD-15705	04:02:16.49	-15:21:29.8	A7	43.0±1.0	45 ⁺⁴ ₋₄	10.02±0.06	7.70±0.05	Galicher16
HIP21547	04:37:36.13	-02:28:24.8	F0	30.0±3.0	23 ⁺³ ₋₃	5.21±0.01	4.77±0.08	Galicher16
HIP22152	04:46:00.58	+76:36:39.8	F7	32.0±2.0	30 ⁺²⁰ ₋₁₀	6.46±0.01	5.33±0.03	Galicher16
HIP22192	04:46:25.75	-28:05:14.8	A3	56.0±1.0	65 ⁺³⁵ ₋₃₅	6.17±0.01	5.73±0.04	Galicher16
HIP22295	04:48:05.17	-80:46:45.2	F7	60.0±1.0	45 ⁺⁴ ₋₄	8.15±0.04	6.99±0.03	Galicher16
HD36652	05:34:09.05	+21:03:39.0	A0	76.0±1.0	125 ⁺²⁰⁰ ₋₇₀	9.7±0.01	8.39±0.05	Galicher16
HD37230	05:37:58.46	+22:27:54.8	A0	472.0±1.0	625 ⁺⁹³⁷⁵ ₋₃₀₀	8.02±0.02	8.48±0.02	Galicher16
WDSJ05574+0002B	05:57:25.23	+00:01:39.6	B9	178.0±2.0	300 ⁺³⁰⁰ ₋₂₀₀	10.2±0.05	6.85±0.03	Galicher16
HD295290	06:40:22.36	-03:31:59.1	F0	19.0±2.0	30 ⁺²⁰ ₋₁₀	9.14±0.07	7.02±0.03	Galicher16
HIP32235	06:43:46.24	-71:58:35.4	G6	57.0±1.0	30 ⁺²⁰ ₋₁₀	9.06±0.05	7.38±0.03	Galicher16
HIP33649	06:59:27.19	+37:05:53.5	M0	351.0±1.0	63 ⁺⁷⁰ ₋₃₀	7.89±0.01	8.02±0.02	Galicher16
TYC1349-1593-1	07:10:11.02	+18:26:22.0	K0	40.0±2.0	30 ⁺⁷⁰ ₋₂₀	9.18±0.08	7.11±0.03	Galicher16
TYC1360-0957-1	07:31:22.06	+15:55:59.9	K5	63.0±1.0	20 ⁺²⁰ ₋₁₀	10.17±0.04	7.58±0.03	Galicher16
HR3504	08:50:45.12	+18:49:55.8	A2	289.0±1.0	625 ⁺⁹³⁷⁵ ₋₃₀₀	6.42±0.01	6.36±0.02	Galicher16
HD80652	09:21:25.49	+16:35:53.9	A5	136.0±1.0	625 ⁺⁹³⁷⁵ ₋₃₀₀	7.02±0.05	6.34±0.02	Galicher16
HR3823	09:35:11.82	-35:49:25.5	F2	65.0±2.0	900 ⁺⁹¹⁰⁰ ₋₃₀₀	6.47±0.01	5.54±0.02	Galicher16
HIP47701	09:43:33.26	+29:58:28.1	A2	49.0±1.0	30 ⁺⁷⁰ ₋₂₀	5.62±0.01	5.44±0.02	Galicher16
HIP48926	09:58:52.27	-35:53:27.5	F1	33.0±14.0	100 ⁺²⁰⁰ ₋₇₀	5.22±0.01	4.50±0.27	Galicher16
BD-212961	09:59:08.42	-22:39:34.6	F2	40.0±1.0	8 ⁺⁵ ₋₃	9.97±0.04	7.49±0.04	Galicher16
HIP50888	10:23:29.30	-38:00:35.4	A8	42.0±453.0	300 ⁺³⁰⁰ ₋₂₀₀	5.33±0.01	4.79±8.89	Galicher16
HIP51386	10:29:42.23	+01:29:28.0	G1	32.0±1.0	50 ⁺⁷⁰ ₋₃₀	6.88±0.01	5.60±0.03	Galicher16
HIP56445	11:34:21.95	+03:03:36.6	F5.5	27.0±13.0	100 ⁺²⁰⁰ ₋₇₀	5.7±0.05	4.78±0.28	Galicher16
HIP58876	12:04:33.73	+66:20:11.7	F8	48.0±1.0	200 ⁺²⁰⁰ ₋₁₀₀	7.91±0.01	6.58±0.02	Galicher16
HIP63584	13:01:46.93	+63:36:36.8	F6	37.0±1.0	600 ⁺⁹⁴⁰⁰ ₋₃₀₀	6.01±0.01	5.05±0.02	Galicher16
HIP66704	13:40:23.23	+50:31:09.9	F7.7	25.0±1.0	65 ⁺³⁵ ₋₃₅	6.32±0.01	5.11±0.02	Galicher16
HIP68593	14:02:31.64	+31:39:39.1	F8	37.0±1.0	2300 ⁺⁷⁷⁰⁰ ₋₃₀₀	7.15±0.01	5.94±0.02	Galicher16
HIP73765	15:04:43.52	+38:36:18.8	F8	49.0±1.0	65 ⁺³⁵ ₋₃₅	7.49±0.01	6.32±0.02	Galicher16
BD+042967	15:07:59.59	+04:15:20.9	K0	37.0±1.0	100 ⁺²⁰⁰ ₋₇₀	9.64±0.05	7.18±0.03	Galicher16
HIP75761	15:28:38.24	+01:50:31.5	A8	40.0±1.0	300 ⁺³⁰⁰ ₋₂₀₀	5.17±0.05	4.78±0.03	Galicher16
HIP77199	15:45:47.60	-30:20:55.7	K2	41.0±1.0	10 ⁺²⁰ ₋₅	9.37±0.02	6.64±0.02	Galicher16
HIP78286	15:59:04.40	+49:52:51.8	F0	49.0±1.0	850 ⁺⁹¹⁵⁰ ₋₃₀₀	6.03±0.01	5.32±0.02	Galicher16
HIP80480	16:25:43.19	+78:57:49.9	F0	42.0±1.0	400 ⁺³⁰⁰ ₋₂₀₀	5.56±0.01	5.00±0.03	Galicher16
HD151044	16:42:27.81	+49:56:11.2	F8	29.0±1.0	3000 ⁺¹³⁰⁰ ₋₁₀₀₀	6.47±0.01	5.17±0.03	Galicher16
HIP82587	16:52:58.06	+31:42:06.0	F0	30.0±2.0	100 ⁺²⁰⁰ ₋₇₀	5.33±0.01	4.54±0.04	Galicher16
HD158352	17:28:49.65	+00:19:50.2	A7	60.0±1.0	600 ⁺⁹⁴⁰⁰ ₋₃₀₀	5.41±0.01	4.88±0.02	Galicher16
HIP87212	17:49:04.29	+50:46:51.9	A2	67.0±2.0	300 ⁺³⁰⁰ ₋₂₀₀	5.02±0.05	4.95±0.03	Galicher16
HD347929	18:07:24.12	+19:42:22.9	K2	15.0±1.0	30 ⁺⁷⁰ ₋₂₀	9.1±0.02	5.99±0.02	Galicher16
HD165780	18:08:1.33	-08:58:58.1	G5	61.0±1.0	100 ⁺²⁰⁰ ₋₇₀	9.59±0.03	7.76±0.04	Galicher16
HIP88945	18:09:21.38	+29:57:06.2	G1	25.0±1.0	200 ⁺⁴⁰⁰ ₋₁₀₀	6.83±0.01	5.39±0.02	Galicher16
HIP91043	18:34:20.11	+18:41:24.2	G2	37.0±1.0	10 ⁺²⁰ ₋₅	7.45±0.04	5.90±0.03	Galicher16
HIP93375	19:01:06.04	-28:42:50.4	G1	63.0±1.0	100 ⁺²⁰⁰ ₋₇₀	8.47±0.01	7.28±0.05	Galicher16
HIP95793	19:29:00.99	+01:57:01.6	A0	61.0±2.0	10 ⁺²⁰ ₋₅	5.78±0.01	5.59±0.05	Galicher16
HIP96313	19:34:58.97	+27:13:31.2	A3	61.0±1.0	10 ⁺²⁰ ₋₅	6.73±0.01	6.13±0.02	Galicher16
HIP97229	19:45:39.95	+07:36:47.4	A3	54.0±1.0	125 ⁺²⁰⁰ ₋₇₀	5.91±0.05	5.47±0.04	Galicher16
HD191616	20:10:43.82	+04:54:49.2	K0	27.0±1.0	50 ⁺⁷⁰ ₋₃₀	9.35±0.02	6.71±0.02	Galicher16
HIP102253	20:43:11.02	+66:39:26.8	A8	43.0±2.0	125 ⁺²⁰⁰ ₋₇₀	5.6±0.01	5.13±0.05	Galicher16
HIP102626	20:47:45.01	-36:35:40.8	K3	44.0±1.0	30 ⁺²⁰ ₋₁₀	9.34±0.09	6.93±0.03	Galicher16
BD+443670	21:00:47.11	+45:30:10.9	F8	61.0±1.0	45 ⁺¹⁰ ₋₁₀	8.83±0.05	7.01±0.03	Galicher16
HIP105860	21:26:26.66	+19:22:32.3	A8	46.0±1.0	125 ⁺²⁰⁰ ₋₇₀	6.06±0.01	5.49±0.03	Galicher16

Table 7 — *Continued*

Target	R.A.	Dec.	Sp. Type	Dist (pc)	Age (Myr)	V (mag)	H (mag)	Survey
HIP105966	21:27:40.05	+27:36:30.9	A1	58.0±2.0	125 ⁺²⁰⁰ ₋₇₀	5.38±0.01	5.37±0.05	Galicher16
HIP107302	21:44:00.97	-14:44:57.7	A7	53.0±1.0	125 ⁺²⁰⁰ ₋₇₀	5.95±0.01	5.46±0.03	Galicher16
HIP107412	21:45:21.90	-12:47:00.1	F5	52.0±1.0	200 ⁺²⁰⁰ ₋₁₀₀	6.67±0.01	5.69±0.03	Galicher16
HIP108809	22:02:32.96	-32:08:01.5	F6.5	30.0±1.0	600 ⁺⁹⁴⁰⁰ ₋₃₀₀	6.63±0.01	5.44±0.04	Galicher16
HIP109901	22:15:35.22	-39:00:50.7	K2	54.0±1.0	50 ⁺⁷⁰ ₋₃₀	9.34±0.04	7.20±0.05	Galicher16
HIP113579	23:00:19.29	-26:09:13.5	G5	32.0±1.0	70 ⁺³⁰ ₋₄₀	7.48±0.01	6.04±0.03	Galicher16
TYC2751-9-1	23:07:24.88	+31:50:14.1	K4	90.0±1.0	30 ⁺⁷⁰ ₋₂₀	10.48±0.04	7.99±0.04	Galicher16
HIP114379	23:09:57.37	+47:57:30.1	G5	25.0±1.0	100 ⁺²⁰⁰ ₋₇₀	7.93±0.05	5.79±0.03	Galicher16
HIP116791	23:40:13.61	-28:21:32.9	F5	106.0±1.0	1400 ⁺⁸⁶⁰⁰ ₋₃₀₀	7.63±0.01	6.50±0.03	Galicher16
V344_And	00:11:22.44	+30:26:58.5	K0	34.1±1.0	118 ⁺¹⁶² ₋₆₈	7.96±0.05	6.26±0.02	Lafreniere07
PW_And	00:18:20.90	+30:57:22.0	K2	30.6±1.0	150 ⁺⁵⁰ ₋₃₀	8.86±0.01	6.51±0.02	Lafreniere07
HD5996	01:02:57.22	+69:13:37.4	G5	25.8±1.0	254 ⁺³⁹⁶ ₋₁₅₄	7.67±0.05	5.98±0.02	Lafreniere07
HD9540	01:33:15.81	-24:10:40.7	K0	19.5±1.0	367 ⁺⁹⁸³ ₋₂₆₇	6.96±0.05	5.27±0.03	Lafreniere07
HD10008	01:37:35.47	-06:45:37.5	G5	23.6±1.0	212 ⁺⁸⁸ ₋₆₂	7.66±0.05	5.90±0.04	Lafreniere07
HD17190	02:46:15.21	+25:38:59.6	K1	25.7±1.0	418 ⁺³⁰⁸² ₋₃₆₈	7.81±0.05	6.00±0.04	Lafreniere07
HD17382	02:48:09.14	+27:04:07.1	K1	22.4±1.0	173 ⁺⁴²⁷ ₋₁₂₃	7.62±0.05	5.69±0.05	Lafreniere07
51_Ari	03:02:26.03	+26:36:33.3	G8	21.2±1.0	1697 ⁺¹⁹⁰³ ₋₈₉₇	6.62±0.01	5.02±0.01	Lafreniere07
HD20367	03:17:40.05	+31:07:37.4	G0	27.1±1.0	86 ⁺⁶⁴ ₋₃₆	6.4±0.01	5.12±0.03	Lafreniere07
V833_Tau	04:36:48.24	+27:07:55.9	K2	17.9±1.0	86 ⁺⁶⁴ ₋₃₆	8.42±0.05	5.40±0.02	Lafreniere07
HD75332	08:50:32.22	+33:17:06.2	F7	28.7±1.0	86 ⁺⁶⁴ ₋₃₆	6.21±0.01	5.03±0.03	Lafreniere07
HD78141	09:07:18.08	+22:52:21.6	K0	21.4±1.0	86 ⁺⁶⁴ ₋₃₆	7.98±0.02	5.92±0.03	Lafreniere07
LQ_Hya	09:32:25.57	-11:11:04.7	K0	18.3±1.0	70 ⁺³⁰ ₋₂₀	7.89±0.1	5.60±0.04	Lafreniere07
HD91901	10:36:30.79	-13:50:35.8	K2	31.6±1.0	499 ⁺⁴⁵⁰¹ ₋₄₄₉	8.75±0.05	6.64±0.04	Lafreniere07
HD93528	10:47:31.16	-22:20:52.9	K0	34.9±1.0	86 ⁺⁶⁴ ₋₃₆	8.39±0.05	6.56±0.03	Lafreniere07
HD96064	11:04:41.47	-04:13:15.9	G4	24.6±1.0	86 ⁺⁶⁴ ₋₃₆	7.64±0.05	5.90±0.04	Lafreniere07
HD97334	11:12:32.35	+35:48:50.7	G0	21.7±1.0	154 ⁺¹⁴⁶ ₋₇₄	6.41±0.05	5.02±0.02	Lafreniere07
HD102195	11:45:42.29	+02:49:17.3	K0	29.0±1.0	707 ⁺⁴²⁹³ ₋₆₀₇	8.06±0.01	6.27±0.03	Lafreniere07
BD+60_1417	12:43:33.28	+60:00:52.7	K0	17.7±1.0	86 ⁺⁶⁴ ₋₃₆	9.37±0.02	7.36±0.02	Lafreniere07
HD113449	13:03:49.65	-05:09:42.5	G5	22.1±1.0	97 ⁺²³ ₋₁₇	7.68±0.05	5.67±0.04	Lafreniere07
HD116956	13:25:45.53	+56:58:13.8	G9	21.9±1.0	223 ⁺²⁷⁷ ₋₁₂₃	7.28±0.01	5.48±0.02	Lafreniere07
HIP69357	14:11:46.17	-12:36:42.4	K1	23.1±1.0	1095 ⁺⁴⁰⁵ ₋₂₉₅	7.95±0.05	5.95±0.02	Lafreniere07
HD125161	14:16:12.16	+51:22:34.7	K1	29.8±2.0	499 ⁺⁴⁵⁰¹ ₋₄₄₉	4.75±0.05	6.32±0.05	Lafreniere07
HD130004	14:45:24.18	+13:50:46.7	K0	19.5±1.0	707 ⁺⁴²⁹³ ₋₆₀₇	7.87±0.01	5.67±0.03	Lafreniere07
HD130322	14:47:32.73	+00:16:53.3	K0	29.8±1.0	1359 ⁺¹⁰⁴¹ ₋₅₈₉	8.04±0.05	6.32±0.03	Lafreniere07
HD139813	15:29:23.59	+80:27:01.0	G5	21.7±1.0	86 ⁺⁶⁴ ₋₃₆	7.31±0.05	5.56±0.03	Lafreniere07
HD141272	15:48:09.46	+01:34:18.3	G8	21.3±1.0	225 ⁺¹¹⁵ ₋₇₅	7.42±0.05	5.61±0.03	Lafreniere07
HD187748	19:48:15.45	+59:25:22.4	G0	28.4±1.0	86 ⁺⁶⁴ ₋₃₆	6.64±0.01	5.32±0.03	Lafreniere07
HIP101262	20:31:32.07	+33:46:33.1	K5	26.2±1.0	223 ⁺⁷⁷⁷ ₋₁₇₃	9.2±0.05	6.64±0.02	Lafreniere07
HD201651	21:06:56.39	+69:40:28.5	K0	32.8±1.0	543 ⁺⁵³⁵⁷ ₋₄₉₃	8.2±0.05	6.41±0.05	Lafreniere07
HD202575	21:16:32.47	+09:23:37.8	K3	16.2±1.0	316 ⁺⁶⁸⁴ ₋₂₁₆	7.88±0.05	5.53±0.02	Lafreniere07
LO_Peg	21:31:01.71	+23:20:07.4	K8	25.1±1.0	150 ⁺⁵⁰ ₋₃₀	9.25±0.06	6.52±0.04	Lafreniere07
HD208313	21:54:45.04	+32:19:42.9	K0	20.3±1.0	316 ⁺⁶⁸⁴ ₋₂₁₆	7.78±0.05	5.68±0.02	Lafreniere07
V383_Lac	22:20:07.03	+49:30:11.8	K1	27.5±1.0	86 ⁺⁶⁴ ₋₃₆	8.58±0.01	6.58±0.03	Lafreniere07
V368_Cep	23:19:26.63	+79:00:12.7	K1	19.7±2.0	86 ⁺⁶⁴ ₋₃₆	7.54±0.01	5.51±0.04	Lafreniere07
HD221503	23:32:49.40	-16:50:44.3	K5	13.9±1.0	282 ⁺⁵¹⁸ ₋₁₈₂	8.61±0.05	5.61±0.03	Lafreniere07
HD_1160	00:15:57.30	+04:15:04.0	A0	103.0±1.0	92 ⁺⁸⁶ ₋₅₆	7.14±0.05	7.01±0.02	Nielsen13
HD_17848	02:49:01.49	-62:48:23.5	A2	50.5±3.0	372 ⁺⁹⁵ ₋₁₀₃	5.25±0.01	5.16±0.08	Nielsen13
HIP_25280	05:24:28.49	-16:58:32.8	A0	68.2±1.0	173 ⁺⁶⁸ ₋₆₇	5.64±0.01	5.68±0.04	Nielsen13
HD_46190	06:27:48.62	-62:08:59.7	A0	83.8±1.0	178 ⁺¹¹⁵ ₋₁₁₃	6.61±0.01	6.39±0.04	Nielsen13
HIP_40916	08:21:00.46	-52:13:40.7	A0	67.2±1.0	119 ⁺⁹⁶ ₋₇₀	6.63±0.01	6.31±0.03	Nielsen13
HIP_45150	09:11:55.63	+05:28:07.1	A9	50.7±1.0	889 ⁺³¹⁴ ₋₂₇₇	6.34±0.01	5.63±0.03	Nielsen13
HIP_54688	11:11:43.76	+14:24:00.6	A5	56.2±1.0	279 ⁺²⁰⁰ ₋₁₇₇	6.3±0.01	5.83±0.04	Nielsen13
HD_118878	13:40:37.65	-44:19:48.8	A0	121.0±1.0	360 ⁺³⁶ ₋₅₁	6.57±0.01	6.35±0.02	Nielsen13
HD_135454	15:16:37.15	-42:22:12.6	B9	172.0±1.0	238 ⁺³⁷ ₋₃₀	6.75±0.01	6.82±0.04	Nielsen13
HIP_78106	15:56:54.11	-33:57:51.3	B9	61.0±1.0	285 ⁺¹²⁰ ₋₁₇₇	5.55±0.01	5.49±0.03	Nielsen13
HD_145964	16:14:28.88	-21:06:27.5	B9	108.0±1.0	254 ⁺⁶⁴ ₋₇₅	6.41±0.01	6.39±0.05	Nielsen13
HIP_79781	16:16:55.30	-03:57:12.1	A9	44.4±1.0	692 ⁺³⁷² ₋₃₈₆	6.16±0.01	5.41±0.03	Nielsen13
HIP_79797	16:17:05.41	-67:56:28.6	A4	52.2±1.0	203 ⁺¹⁶⁹ ₋₁₃₂	5.94±0.01	5.68±0.05	Nielsen13
HIP_79881	16:18:17.90	-28:36:50.5	A0	41.3±3.0	107 ⁺⁹⁹ ₋₆₃	4.78±0.01	4.94±0.08	Nielsen13

Table 7 — *Continued*

Target	R.A.	Dec.	Sp. Type	Dist (pc)	Age (Myr)	V (mag)	H (mag)	Survey
HIP_81650	16:40:44.40	-51:28:41.7	A9	49.4±1.0	809 ⁺³²⁴ ₋₃₀₆	6.29±0.01	5.52±0.03	Nielsen13
HIP_85038	17:22:47.89	-58:28:23.7	A5	62.0±1.0	315 ⁺²⁹⁰ ₋₂₀₇	6.83±0.05	6.30±0.04	Nielsen13
HIP_110935	22:28:37.67	-67:29:20.6	A3	43.1±2.0	457 ⁺¹⁷⁸ ₋₁₉₇	5.56±0.01	5.14±0.05	Nielsen13
HIP_14551	03:07:50.80	-27:49:52.1	A5	54.6±2.0	45 ⁺⁴ ₋₄	6.17±0.01	5.85±0.05	Vigan12
HIP_15648	03:21:26.60	+43:19:46.7	A3	46.2±1.0	125 ⁺⁷⁵ ₋₂₅	4.95±0.01	4.86±0.02	Vigan12
HIP_23296	05:00:39.80	-02:03:57.7	A8	49.6±1.0	125 ⁺⁷⁵ ₋₂₅	6.32±0.05	5.62±0.02	Vigan12
HIP26624	05:39:31.20	-03:33:52.9	A8	42.6±2.0	125 ⁺⁷⁵ ₋₂₅	5.97±0.01	5.36±0.05	Vigan12
HIP_32938	06:51:42.40	-36:13:49.0	A3	55.2±1.0	125 ⁺⁷⁵ ₋₂₅	5.94±0.01	5.53±0.03	Vigan12
HIP_34782	07:12:04.10	-30:49:16.9	A8	47.6±1.0	125 ⁺⁷⁵ ₋₂₅	6.08±0.01	5.46±0.04	Vigan12
HIP_42334	08:37:52.20	-26:15:18.0	A0	71.1±1.0	125 ⁺⁷⁵ ₋₂₅	5.27±0.05	5.35±0.04	Vigan12
HIP_53771	11:00:08.30	-51:49:04.1	A3	61.1±1.0	125 ⁺⁷⁵ ₋₂₂₅	6.14±0.01	5.78±0.03	Vigan12
HIP_57013	11:41:19.80	-43:05:44.4	A0	65.5±2.0	125 ⁺⁷⁵ ₋₂₅	5.53±0.01	5.51±0.05	Vigan12
HIP_60595	12:25:11.80	-11:36:38.1	A1	70.5±1.0	125 ⁺⁷⁵ ₋₂₅	5.93±0.01	5.91±0.02	Vigan12
HIP_66634	13:39:30.40	+52:55:16.4	A3	53.6±1.0	125 ⁺⁷⁵ ₋₂₅	5.46±0.01	5.20±0.02	Vigan12
HIP_78078	15:56:33.40	-14:49:46.0	A2	51.1±2.0	125 ⁺⁷⁵ ₋₂₅	6.12±0.01	5.39±0.05	Vigan12
HIP_104365	21:08:33.60	-21:11:37.2	A0	55.1±2.0	125 ⁺⁷⁵ ₋₂₅	5.28±0.05	5.33±0.05	Vigan12
HIP_2729	00:34:51.20	-61:54:58.0	K4	43.9±1.0	45 ⁺⁴ ₋₄	9.6±0.06	6.72±0.03	Biller13
CD-53_544	02:41:46.80	-52:59:52.0	K6	42.0±1.0	45 ⁺⁴ ₋₄	10.28±0.03	6.93±0.03	Biller13
AF_Hor	02:41:47.30	-52:59:31.0	M2	42.0±1.0	45 ⁺⁴ ₋₄	12.21±0.05	7.85±0.03	Biller13
HIP_17695	03:47:23.34	-01:58:19.9	M3	16.1±1.0	150 ⁺⁵⁰ ₋₃₀	11.54±0.05	7.17±0.05	Biller13
LP_776-25	04:52:24.40	-16:49:22.0	M3	16.0±1.0	150 ⁺⁵⁰ ₋₃₀	11.64±0.05	7.15±0.03	Biller13
GJ_2036B	04:53:30.50	-55:51:32.0	M3	11.1±1.0	150 ⁺⁵⁰ ₋₃₀	13.92±0.04	7.24±0.03	Biller13
GJ_182	04:59:34.80	+01:47:00.7	M0	25.9±1.0	23 ⁺³ ₋₃	10.11±0.05	6.45±0.03	Biller13
HIP_23309	05:00:47.10	-57:15:25.5	M0	26.8±1.0	23 ⁺³ ₋₃	9.98±0.04	6.43±0.03	Biller13
BD-21_1074A	05:06:49.90	-21:35:09.0	M1	18.0±1.0	23 ⁺³ ₋₃	10.41±0.02	6.39±0.05	Biller13
HIP_26369	05:36:55.10	-47:57:48.0	K6	25.6±1.0	150 ⁺⁵⁰ ₋₃₀	9.86±0.05	6.83±0.04	Biller13
CD-35_2722	06:09:19.20	-35:49:31.0	M1	24.0±1.0	150 ⁺⁵⁰ ₋₃₀	11.08±0.07	7.28±0.03	Biller13
GSC_8894-0426	06:25:56.10	-60:03:27.0	M3	22.0±1.0	150 ⁺⁵⁰ ₋₃₀	12.32±0.09	7.47±0.04	Biller13
TWA_6	10:18:28.80	-31:50:02.0	M0	77.0±1.0	10 ⁺³ ₋₃	11.45±0.07	8.18±0.04	Biller13
BD+1_2447	10:28:55.50	+00:50:28.0	M2	7.1±1.0	150 ⁺⁵⁰ ₋₃₀	9.65±0.0	5.61±0.03	Biller13
TWA_14	11:13:26.50	-45:23:43.0	M0	95.9±1.0	10 ⁺³ ₋₃	12.48±0.08	8.73±0.04	Biller13
TWA_13A	11:21:17.20	-34:46:46.0	M1	55.6±1.0	10 ⁺³ ₋₃	11.46±0.05	7.68±0.05	Biller13
TWA_8A	11:32:41.20	-26:51:56.0	M3	47.0±1.0	10 ⁺³ ₋₃	12.23±0.06	7.66±0.04	Biller13
TWA_9B	11:48:23.70	-37:28:48.0	M1	46.8±1.0	10 ⁺³ ₋₃	14.0±0.05	9.38±0.02	Biller13
TWA_25	12:15:30.80	-39:48:42.0	M1	51.0±1.0	10 ⁺³ ₋₃	11.16±0.08	7.50±0.04	Biller13
TWA_20	12:31:38.10	-45:58:59.0	M3	77.5±1.0	10 ⁺³ ₋₃	13.24±0.13	8.69±0.06	Biller13
TWA_10	12:35:04.20	-41:36:39.0	M2	52.0±1.0	10 ⁺³ ₋₃	13.05±0.12	8.48±0.04	Biller13
HIP_81084	16:33:41.60	-09:33:11.9	M0	30.7±1.0	150 ⁺⁵⁰ ₋₃₀	11.28±0.03	7.78±0.05	Biller13
HD_15555_C	17:17:31.30	-66:57:05.0	M3	31.4±1.0	23 ⁺³ ₋₃	12.82±0.05	7.92±0.04	Biller13
TYC_9073-0762-1	18:46:52.60	-62:10:36.0	M1	54.0±1.0	23 ⁺³ ₋₃	11.83±0.02	8.05±0.04	Biller13
CD-31_16041	18:50:44.50	-31:47:47.0	K8	51.0±1.0	23 ⁺³ ₋₃	11.19±0.01	7.67±0.05	Biller13
1RXS_J195602.8-320720	19:56:02.94	-32:07:18.7	M4	57.7±1.0	23 ⁺³ ₋₃	13.23±0.04	8.34±0.04	Biller13
2MASS_J19560438-3207376	19:56:04.37	-32:07:37.7	M0	57.7±1.0	23 ⁺³ ₋₃	11.59±0.02	8.03±0.04	Biller13
GJ_803	20:45:09.50	-31:20:27.1	M1	9.9±1.0	23 ⁺³ ₋₃	8.63±0.05	4.83±0.02	Biller13
HIP_107345	21:44:30.10	-60:58:38.0	M0	43.6±1.0	45 ⁺⁴ ₋₄	11.63±0.09	8.09±0.02	Biller13
CP-72_2713	22:42:49.00	-71:42:21.0	K7	36.0±1.0	23 ⁺³ ₋₃	10.56±0.08	7.12±0.05	Biller13
HIP_112312	22:44:57.80	-33:15:01.0	M4	23.3±1.0	23 ⁺³ ₋₃	12.11±0.08	7.15±0.03	Biller13
TX_PsA	22:45:00.00	-33:15:26.0	M5	20.0±1.0	23 ⁺³ ₋₃	13.36±0.05	8.06±0.03	Biller13
BD-13_6424	23:32:30.90	-12:15:52.0	M0	28.0±1.0	23 ⁺³ ₋₃	10.64±0.04	6.77±0.04	Biller13
G_272-43	01:33:58.00	-17:38:23.5	M3.5	16.0±1.0	54 ⁺²⁴⁶ ₋₄₄	13.04±0.06	8.24±0.02	Bowler15
GJ_3136	02:08:53.60	+49:26:56.6	M4.0	15.0±1.0	150 ⁺⁵⁰ ₋₃₀	12.45±0.06	7.81±0.02	Bowler15
LP_353-51	02:23:26.64	+22:44:06.9	M0.5	28.7±1.0	23 ⁺³ ₋₃	11.25±0.03	7.56±0.02	Bowler15
1RXS_J023138.7+445640	02:31:39.27	+44:56:38.8	M4.4	16.0±1.0	109 ⁺¹⁹¹ ₋₆₉	14.5±0.05	9.40±0.02	Bowler15
G_75-35	02:41:15.11	-04:32:17.7	M4.0	16.0±1.0	54 ⁺²⁴⁶ ₋₄₄	13.79±0.05	8.58±0.06	Bowler15
GJ_3287	04:27:41.30	+59:35:16.7	M3.8	22.5±1.0	102 ⁺¹⁹⁸ ₋₆₇	14.44±0.05	9.43±0.02	Bowler15
LP_834-32	04:35:36.19	-25:27:34.7	M3.5	15.0±1.0	150 ⁺⁵⁰ ₋₃₀	12.41±0.01	7.65±0.03	Bowler15
1RXS_J055446.0+105559	05:54:45.74	+10:55:57.1	M3.0	25.4±2.0	54 ⁺⁹⁶ ₋₃₄	12.52±0.04	8.21±0.05	Bowler15
GJ_3371	05:59:37.75	+58:35:35.1	M1.0	13.5±1.0	400 ⁺⁵⁰ ₋₅₀	10.26±0.05	6.42±0.02	Bowler15
AP_Col	06:04:52.16	-34:33:36.1	M5.0	8.4±1.0	40 ⁺⁵ ₋₅	12.96±0.02	7.18±0.02	Bowler15

Table 7 — Continued

Target	R.A.	Dec.	Sp. Type	Dist (pc)	Age (Myr)	V (mag)	H (mag)	Survey
2MASS_J06180730+7506032	06:18:07.30	+75:06:03.3	M2.0	18.0±1.0	54 ⁺²⁴⁶ ₋₄₄	11.4±0.03	7.39±0.02	Bowler15
GJ_3395	06:31:01.16	+50:02:48.6	M1.0	28.0±1.0	54 ⁺⁹⁶ ₋₃₄	11.06±0.04	7.25±0.02	Bowler15
G_108-36	06:51:59.01	+03:12:55.3	M2.5	22.2±2.0	54 ⁺⁹⁶ ₋₃₄	13.02±0.02	8.57±0.05	Bowler15
1RXS_J073829.3+240014	07:38:29.52	+24:00:08.8	M3.5	18.9±1.0	77 ⁺²²³ ₋₅₇	12.98±0.03	8.35±0.02	Bowler15
G_161-71	09:44:54.22	-12:20:54.4	M5.0	8.0±1.0	40 ⁺⁵ ₋₅	13.65±0.18	7.92±0.02	Bowler15
GJ_3577	09:59:18.80	+43:50:25.6	M3.3	24.9±1.0	86 ⁺²¹⁴ ₋₆₁	13.89±0.02	9.13±0.02	Bowler15
GJ_3578	09:59:20.94	+43:50:25.9	M3.8	24.9±1.0	86 ⁺²¹⁴ ₋₆₁	14.23±0.03	9.33±0.02	Bowler15
G_196-3	10:04:21.49	+50:23:13.6	M2.5	24.4±1.0	38 ⁺¹¹² ₋₂₈	11.67±0.03	7.41±0.02	Bowler15
GJ_3629	10:51:20.60	+36:07:25.6	M3.0	32.3±1.0	86 ⁺²¹⁴ ₋₆₁	13.46±0.05	8.82±0.02	Bowler15
GJ_3639	11:03:10.00	+36:39:08.5	M3.5	24.0±1.0	86 ⁺²¹⁴ ₋₆₁	13.75±0.07	8.91±0.02	Bowler15
NLTT_26114	11:03:21.25	+13:37:57.1	M4.0	15.4±1.0	86 ⁺²¹⁴ ₋₆₁	12.99±0.04	8.18±0.05	Bowler15
NLTT_26359	11:07:27.73	-19:17:29.4	K5	18.7±1.0	54 ⁺²⁴⁶ ₋₄₄	10.38±0.05	6.85±0.06	Bowler15
2MASS_J11240434+3808108	11:24:04.35	+38:08:10.9	M4.5	20.3±1.0	530 ⁺⁴⁰ ₋₄₀	14.55±0.01	9.39±0.02	Bowler15
G_10-52	11:48:35.49	+07:41:40.4	M3.5	20.7±2.0	86 ⁺²¹⁴ ₋₆₁	13.64±0.07	8.88±0.02	Bowler15
LP_734-34	12:10:28.34	-13:10:23.5	M4.5	16.0±1.0	54 ⁺²⁴⁶ ₋₄₄	13.8±0.02	8.68±0.03	Bowler15
1RXS_J124147.5+564506	12:41:47.37	+56:45:13.8	M3.0	30.0±1.0	530 ⁺⁴⁰ ₋₄₀	13.5±0.04	8.85±0.02	Bowler15
LHS_2613	12:42:49.96	+41:53:47.0	M4.0	10.6±1.0	40 ⁺⁵ ₋₅	12.42±0.02	7.50±0.03	Bowler15
LHS_2672	13:02:47.52	+41:31:09.9	M3.5	17.0±1.0	5477 ⁺⁴⁵²³ ₋₂₄₇₇	12.96±0.09	8.42±0.02	Bowler15
GJ_1167	13:09:34.95	+28:59:06.6	M3.5	11.5±1.0	45 ⁺¹⁰ ₋₁₀	14.08±0.01	8.91±0.03	Bowler15
LHS_2686	13:10:12.69	+47:45:19.0	M4.5	13.1±1.0	223 ⁺²⁷⁷ ₋₁₂₃	14.59±0.03	8.99±0.02	Bowler15
2MASS_J13233804-2554449	13:23:38.05	-25:54:45.0	M3.5	24.0±1.0	54 ⁺²⁴⁶ ₋₄₄	12.89±0.06	8.07±0.05	Bowler15
2MASS_J13292408-1422122	13:29:24.08	-14:22:12.3	M3.5	21.0±1.0	54 ⁺⁹⁶ ₋₃₄	13.13±0.04	8.45±0.05	Bowler15
2MASS_J14124864-1629561	14:12:48.64	-16:29:56.1	M3.0	27.0±1.0	54 ⁺²⁴⁶ ₋₄₄	13.25±0.03	8.85±0.02	Bowler15
GQ_Vir	14:13:04.92	-12:01:26.3	M4.5	10.0±1.0	54 ⁺²⁴⁶ ₋₄₄	13.89±0.05	8.45±0.04	Bowler15
2MASS_J14442809-0424078	14:44:28.10	-04:24:07.8	M2.0	29.0±1.0	530 ⁺⁴⁰ ₋₄₀	13.78±0.01	9.12±0.03	Bowler15
2MASS_J15323737+4653048	15:32:37.38	+46:53:04.9	M1.0	33.0±1.0	54 ⁺²⁴⁶ ₋₄₄	11.12±0.11	7.69±0.02	Bowler15
NLTT_40561	15:33:50.62	+25:10:10.6	M3.5	29.1±2.0	86 ⁺²¹⁴ ₋₆₁	14.6±0.05	9.82±0.02	Bowler15
GJ_669_B	17:19:52.98	+26:30:02.6	M4.5	11.8±1.0	750 ⁺¹⁵⁰ ₋₁₅₀	13.3±0.01	7.64±0.03	Bowler15
GJ_669_A	17:19:54.22	+26:30:03.0	M3.5	11.7±1.0	750 ⁺¹⁵⁰ ₋₁₅₀	11.34±0.02	6.71±0.03	Bowler15
LHS_3321	17:43:55.95	+43:22:44.1	M2.5	9.5±1.0	4000 ⁺⁶⁰⁰⁰ ₋₂₄₀₀	10.49±0.01	6.22±0.02	Bowler15
G_227-22	18:02:16.60	+64:15:44.6	M5.0	8.5±1.0	530 ⁺⁴⁰ ₋₄₀	13.37±0.05	7.96±0.02	Bowler15
LP_390-16	18:13:06.58	+26:01:51.9	M4.5	17.2±1.0	109 ⁺¹⁹¹ ₋₆₉	12.77±0.05	8.31±0.03	Bowler15
NLTT_48651	20:04:30.78	-23:42:01.9	M4.5	10.0±1.0	150 ⁺⁵⁰ ₋₃₀	13.06±0.05	8.01±0.05	Bowler15
2MASS_J20284361-1128307	20:28:43.62	-11:28:30.8	M3.5	18.8±1.0	40 ⁺⁵ ₋₅	12.47±0.02	7.76±0.03	Bowler15
GJ_4186_B	21:16:03.79	+29:51:46.0	M3.3	19.3±1.0	86 ⁺²¹⁴ ₋₆₁	14.0±0.05	8.66±0.02	Bowler15
GJ_4274	22:23:06.97	-17:36:25.0	M4.0	7.3±1.0	223 ⁺²⁷⁷ ₋₅₇	13.3±0.03	7.64±0.05	Bowler15
2MASS_J22581643-1104170	22:58:16.44	-11:04:17.1	M2.7	31.1±1.0	77 ⁺²²³ ₋₅₇	12.94±0.01	8.47±0.02	Bowler15
GJ_4337_A	23:29:23.46	+41:28:06.9	M3.5	14.9±2.0	77 ⁺²²³ ₋₅₇	12.13±0.01	7.33±0.02	Bowler15
1RXS_J235133.3+312720	23:51:33.67	+31:27:23.0	M2.0	50.0±1.0	150 ⁺⁵⁰ ₋₃₀	13.6±0.06	9.17±0.02	Bowler15
1RXS_J235452.2+383129	23:54:51.47	+38:31:36.3	M4.0	15.9±1.0	86 ⁺²¹⁴ ₋₆₁	13.18±0.06	8.35±0.02	Bowler15
G_158-8	23:55:55.13	-13:21:23.8	M2.5	19.0±1.0	40 ⁺⁵ ₋₅	13.37±0.09	8.70±0.03	Bowler15
FK_Psc	00:23:34.70	+20:14:29.0	K7.5	59.7±1.0	23 ⁺³ ₋₃	10.84±0.08	7.50±0.02	Brandt14
BD+30_397B	02:27:28.00	+30:58:41.0	M0	40.0±1.0	23 ⁺³ ₋₃	12.55±0.05	8.14±0.03	Brandt14
HIP17248	03:41:37.30	+55:13:07.0	M0.5	35.2±1.0	45 ⁺¹⁰ ₋₁₀	11.25±0.03	7.65±0.03	Brandt14
HIP37288	07:39:23.00	+02:11:01.0	K7	14.6±1.0	250 ⁺⁵⁰ ₋₅₀	9.59±0.05	6.09±0.04	Brandt14
FP_Cnc	08:08:56.40	+32:49:11.0	K7	20.7±1.0	45 ⁺¹⁰ ₋₁₀	9.99±0.04	6.58±0.02	Brandt14
AD_Leo	10:19:36.30	+19:52:12.0	M3	4.7±1.0	190 ⁺⁵⁰ ₋₅₀	9.52±0.0	4.84±0.02	Brandt14
EE_Leo	10:50:52.00	+06:48:29.0	M5	6.8±1.0	250 ⁺⁵⁰ ₋₅₀	11.68±0.0	6.71±0.05	Brandt14
TYC_4943-192-1	12:15:18.40	-02:37:28.0	M0	30.2±1.0	150 ⁺⁵⁰ ₋₃₀	11.37±0.02	8.00±0.02	Brandt14
HIP114066	23:06:04.80	+63:55:34.0	M0.3	24.5±1.0	150 ⁺⁵⁰ ₋₃₀	10.89±0.06	7.17±0.04	Brandt14
2MASS_J00281434-3227556	00:28:13.50	-32:28:01.5	F2	39.0±1.0	10 ⁺²⁰ ₋₅	15.23±0.0	9.56±0.03	Galicher16
HIP9291	01:59:23.51	+58:31:16.1	M4.0	12.0±1.0	100 ⁺²⁰⁰ ₋₇₀	12.15±0.03	7.22±0.06	Galicher16
HIP12545	02:41:25.89	+05:59:18.4	K6	41.0±1.0	23 ⁺³ ₋₃	10.27±0.07	7.23±0.03	Galicher16
UCAC4_336-004233	03:41:17.23	-22:52:30.9	M2	63.0±2.0	45 ⁺⁴ ₋₄	13.18±0.05	9.30±0.02	Galicher16
2MASS_J06131330-2742054	06:13:13.31	-27:42:05.5	M3.5	17.0±1.0	50 ⁺⁷⁰ ₋₃₀	12.3±0.03	7.43±0.07	Galicher16
2MASS_J07065772-5353463	07:06:59.10	-53:53:47.0	M0	50.0±1.0	10 ⁺²⁰ ₋₅	11.4±0.05	7.90±0.05	Galicher16
CPD-64887	08:27:09.57	-65:04:42.7	K2	21.0±1.0	10 ⁺²⁰ ₋₅	9.67±0.03	6.61±0.02	Galicher16
2MASS_J11200609-1029468	11:20:06.51	-10:29:43.4	M3	20.0±1.0	100 ⁺²⁰⁰ ₋₇₀	11.25±0.04	7.21±0.05	Galicher16
WACK_3672	17:19:41.80	-46:15:24.0	M2	38.0±2.0	15 ⁺⁵ ₋₅	12.93±0.05	8.02±0.03	Galicher16

Table 7 — *Continued*

Target	R.A.	Dec.	Sp. Type	Dist (pc)	Age (Myr)	V (mag)	H (mag)	Survey
GSC07396-00759	18:14:22.08	-32:46:10.1	M1	75.0±1.0	23 ⁺³ ₋₃	12.78±0.05	8.77±0.04	Galicher16
HIP92871	18:55:27.41	+08:24:09.0	M3.0	12.0±1.0	200 ⁺⁵⁰ ₋₅₀	10.19±0.05	5.68±0.02	Galicher16
2MASSJ19233820-4606316	19:23:38.20	-46:06:31.6	M0	66.0±1.0	10 ⁺²⁰ ₋₅	11.87±0.05	8.44±0.03	Galicher16
2MASSJ20013718-3313139	20:01:37.18	-33:13:14.0	M1	70.0±1.0	10 ⁺²⁰ ₋₅	12.32±0.2	8.46±0.05	Galicher16
1RXS_J200556.1-321651	20:05:56.10	-32:16:51.5	M1.5	50.0±1.0	23 ⁺³ ₋₃	12.00±0.05	8.16±0.03	Galicher16
2MASS_J21044799-0418264	21:04:47.00	-04:18:32.0	M1.5	63.0±1.0	100 ⁺²⁰⁰ ₋₇₀	14.31±0.01	9.29±0.02	Galicher16
GSC06354-00357	21:10:05.04	-19:20:09.7	M5	20.0±1.0	12 ⁺¹⁰ ₋₄	11.66±0.1	7.45±0.03	Galicher16
TYC221113091	22:00:41.60	+27:15:13.6	M0	33.0±1.0	10 ⁺²⁰ ₋₅	11.37±0.04	7.95±0.02	Galicher16
HIP108706	22:01:13.13	+28:18:24.9	M4	9.0±1.0	100 ⁺²⁰⁰ ₋₇₀	12.01±0.05	7.03±0.03	Galicher16
HIP113001	22:53:06.00	+07:28:19.1	M0	55.0±1.0	30 ⁺⁷⁰ ₋₂₀	11.36±0.05	8.14±0.04	Galicher16
HIP116003	23:30:13.44	-20:23:27.5	M2	15.0±1.0	23 ⁺³ ₋₃	11.11±0.05	6.61±0.04	Galicher16
YZ_CMi	07:44:40.17	+03:33:08.8	M4.5	5.9±1.0	49 ⁺¹ ₋₁	11.23±0.05	6.01±0.04	Lafreniere07
HIP65016	13:19:40.12	+33:20:47.5	M1.5	17.4±1.0	707 ⁺⁴²⁹³ ₋₆₀₇	10.6±0.01	6.64±0.03	Lafreniere07
HIP67092	13:45:05.34	-04:37:13.2	K5	25.7±1.0	707 ⁺⁴²⁹³ ₋₆₀₇	10.51±0.05	7.33±0.04	Lafreniere07
EW_Dra	16:16:45.31	+67:15:22.5	M3	10.7±1.0	316 ⁺⁶⁸⁴ ₋₂₁₆	10.61±0.04	6.30±0.02	Lafreniere07
V2306_Oph	16:30:18.06	-12:39:45.3	M3.5	4.3±1.0	707 ⁺⁴²⁹³ ₋₆₀₇	10.07±0.0	5.37±0.04	Lafreniere07
HIP87322	17:50:34.03	-06:03:01.0	M0	21.9±1.0	707 ⁺⁴²⁹³ ₋₆₀₇	10.15±0.05	6.70±0.03	Lafreniere07
GT_Peg	22:51:53.54	+31:45:15.2	M3	14.2±1.0	244 ⁺⁵⁶ ₋₄₄	11.66±0.05	7.13±0.02	Lafreniere07
IL_Aqr	22:53:16.73	-14:15:49.3	M4	4.7±2.0	707 ⁺⁴²⁹³ ₋₆₀₇	10.19±0.0	5.35±0.05	Lafreniere07

Note. — References: Lafrenière et al. (2007); Vigan et al. (2012); Biller et al. (2013); Nielsen et al. (2013); Brandt et al. (2014); Bowler et al. (2015); Galicher et al. (2016)